Title: Transfer learning Gaussian process regression surrogate model with explainability for structural reliability analysis under variation in uncertainties

Authors: Taisei SAIDA[a*] and Mayuko NISHIO[b]

[a] Graduate student, Department of Engineering Mechanics and Energy, University of Tsukuba

[b] Ph.D., Associate professor, Department of Engineering Mechanics and Energy, University of Tsukuba (ORCID number: 0000-0003-1079-2577)

* Corresponding author

Email: saida.taisei.tj@alumni.tsukuba.ac.jp

Address: 1-1-1 Tennodai, Tsukuba 305-8573, Japan

Tel: +81-29-853-6192

Abstract:

In this paper, a Gaussian process regression surrogate model with transfer learning (TL-GPRSM) is introduced to reduce the computational cost of structural reliability analysis by using the input–output relationship of the source analysis having similarities with that of the target analysis. In addition, automatic relevance determination (ARD) is introduced for providing the explainability of the constructed model and confidence assurance of transfer learning. Two verifications were conducted: (i) the surrogate modeling of the live-load performance analysis of a steel bridge with corrosion by applying the source analysis in the undamaged condition and (ii) seismic performance

---

ANN: Artificial neural network; ARD: Automatic relevance determination; COV: Coefficient of variation; DoE: Design of experiments; DOF: Degree of freedom; FE: finite element; GP: Gaussian process; GPR: Gaussian process regression; KS: Kolmogorov—Smirnov; L-BFGS: Limited-memory Broyden–Fletcher–Goldfarb–Shanno; LHS: Latin hypercube sampling; MC: Monte Carlo; RMSPE: Root mean square percent error; TL-GPRSM: Gaussian process regression surrogate model with transfer learning

analysis of a bridge pier, which required nonlinear time-history analyses for various earthquake loads. The results showed that TL-GPRSM was especially effective in surrogate modeling of the performance analysis with linear numerical calculations. Moreover, it was shown that the effectiveness of transfer learning in each modeling and explainability of the constructed model could be discussed based on the contributions of the model parameters estimated through ARD.

Keywords: surrogate model, Gaussian process regression, transfer learning, explainability, Monte Carlo calculation, structural reliability analysis

1. Introduction

Structural performance evaluation requires reliability analysis wherein the limit state capacity is statistically derived. It is useful to evaluate the performances of existing structures by considering the actual structure conditions to develop maintenance plans or implement reinforcement/retrofit activities in disaster events. Statistical performance analysis requires the consideration of the uncertainties of the structural properties using Monte Carlo (MC) calculations. The MC calculations require several to ten thousands of numerical calculations with a random sampling of the input parameter space. In modeling an existing structure with deteriorations or damages, a detailed model is required to represent the damage to the structural member; therefore, the number of model parameters becomes large. Moreover, the properties to consider the uncertainties due to the deterioration or damage should be included in addition to the uncertainties of the nominal model properties. In the case of performance evaluation under a disaster load such as an earthquake load, the MC calculations of multiple input load cases should be combined to consider the input load uncertainty. Therefore, high calculation effort is required to assess the structural performance.

The surrogate model is a regression model that alternates the numerical analysis constructed using training data created through design of experiments (DoE) sampling of uncertain input parameters.

The total cost of MC calculation can be reduced if a small amount of training data can appropriately represent the input–output relationship of the target numerical analysis. Numerous studies have been conducted on the application of the surrogate model to structural reliability analysis. The first application of surrogate model for the structural reliability analysis was shown by Bucher and Bourgund [1], where the performance function was approximated by the response surface method (RSM). The RSM has then been improved in many approaches, e.g., in studies by Kim et al. [2] and Zhao et al. [3]. Recently, support vector machine [4,5], polynomial chaos expansion [6,7], and artificial neural network (ANN) [8–10] are often adopted for surrogate modeling, and their effectiveness has been demonstrated. For instance, Marelli and Sudret [7] showed that the polynomial chaos expansion with active learning could construct surrogate models for structural analysis at low computational cost. The applicability of Gaussian process regression (GPR) to surrogate modeling has often been validated [11–14]. GPR [15] is a nonparametric regression method and does not require the determination of the model configuration; moreover, the number of hyperparameters required for the estimation is small, and it can be applied to nonlinear input–output relationships. For instance, Su et al. [12] conducted surrogate modeling by using GPR for the reliability analysis of bridges through finite element (FE) analysis. It was shown to be more efficient and accurate than the polynomial function-based response surface method. Avendaño et al. [14] constructed a GPR surrogate model that effectively predicts wind turbine loads with accuracy of 4% error or less. Adaptive learning method for GPR [16–22] have also been studied for efficient surrogate modeling of the structural reliability analysis, as surveyed by Moustapha et al. [23]. Adaptive learning is the method of incorporating additional learning points into the training data by evaluating the learning function. Some studies, e.g., EGRA by Bichon et al. [16] and AK-MCS by Echard et al. [17], successfully reduced the computational cost of surrogate modeling by implement adaptive sampling to the GPR. Since the AK-MCS was presented, Adaptive Kriging has been studied actively, e.g., AK-IS by Echard et al. [21] and AK-SS by Huang et al. [22]. Many studies on

surrogate modeling have been conducted, although most of them can be applied only to target calculations. However, evaluations through numerical calculations to support decision-making in the engineering field require many similar calculations. The use of the surrogate model in such scenarios will require new training data for the same modeling procedure for each calculation. In other words, a surrogate model and its outputs cannot be used to construct other surrogate models.

Transfer learning (TL) is a machine learning technique in which the knowledge learned in a problem is utilized in the target problem [24]. TL is expected to be applicable to the surrogate modeling of a target numerical calculation that shows any similarity to the source numerical calculation for which a surrogate model is already available; this approach may reduce the computational costs of constructing new surrogate models. Some cases require the repetition of numerical calculations for evaluations in the civil structural engineering field. For instance, when the target calculation is the performance analysis of an existing structure with damages, the surrogate model of the numerical calculation for the initial undamaged condition is expected to be used as the source in the TL. The other is the seismic performance analysis of a structure considering various input earthquake loads. Once a surrogate model for an input earthquake load is constructed, it can be used to construct the surrogate models for other earthquake loads with similar characteristics. If the TL works effectively in these cases, the total computational cost of the structural performance evaluation is expected to be reduced.

Some previous studies have used TL in surrogate modeling. Xiong et al. applied TL to the deep learning model for the thermal analysis of spacecraft [25]. Kaya and Hajimirza applied ANN with TL to the optimization problem of thin-film multilayer solar cells [26]. Tian et al. used TL to construct the variable-fidelity surrogate model with a deep neural network for the buckling analysis of a composite shell with seven design variables and a hierarchical reinforced shell with nine design variables [27]. In all verifications, the prediction errors of the constructed surrogate models that used TL were significantly reduced. However, the studies [25–27] in which TL was used for the surrogate

model assumed that the source and target data in TL are similar from the beginning of the process. In TL, the negative transfer problem is known to occur in some cases. Negative transfer refers to the issue wherein the performance of a machine learning model decreases owing to TL when the similarity between the source and target data, i.e., the input–output relationships between the source and target numerical calculations, is low [24]. For the use of TL with confidence, the possibility of this negative transfer must be considered when it is generally unknown whether the source and target numerical calculations are similar to each other.

In the engineering field, it is generally required to explain the results of physics numerical calculations for their appropriate use, i.e., provide explanations for the results from the viewpoint of validity of the modeling; this requirement applies to surrogate models as well. The issue in most machine learning techniques, which are applicable to surrogate modeling, is that the training and prediction process is a black box. In the structural performance analysis using surrogate models, it is essential to know which uncertainties of the structural properties contribute significantly to the demand output to provide the explainability of the surrogate model. A previous study mentioned the necessity of demonstrating the explainability of the surrogate model. Golparvar et al. [28] constructed a surrogate model for predicting the offshore wind power using GPR with an automatic relevance determination (ARD) kernel, which can estimate the contributions to the input parameters by the hyperparameters in the ARD kernel. The ARD kernel [29,30] is the kernel function to represent the correlation function in the Gaussian process (GP) model, which can assign different weights to each input dimension, and the corresponding length-scale is larger for input dimensions that are irrelevant to the output. Wipf and Nagarajan [30] showed that ARD can be applied to the linear model estimation problem, where the inputs are sparse relative to the output, while retaining the estimation accuracy. Owing to this feature, it is expected that the construction of GPR surrogate models with an ARD kernel can estimate the parameter contribution to the output. However, very few studies have provided the explainability of the use of a machine learning technique to surrogate

122 modeling, especially in the structural engineering field. Furthermore, no study has considered both
123 TL and explainability in surrogate models.
124 This paper develops surrogate modeling using GPR with TL (TL-GPRSM). GPR is also applicable to
125 the surrogate modeling of structural performance analysis, because it can deal with nonlinear input–
126 output relationships that may possibly emerge in the required structural analysis. In addition, as GPR
127 is a nonparametric method, the number of model parameters to be determined can be relatively low
128 when compared with that of other regression methods. Here, TL reduces the computational cost of
129 surrogate modeling for structural performance analysis by considering the similarity in the input–
130 output relationships in the numerical analysis. We also propose the use of the ARD kernel for
131 providing the explainability of the constructed surrogate model and confidence assurance of TL. The
132 appropriately estimated ARD kernel hyperparameters are expected to be useful in evaluating the
133 degree of the TL effect in each target surrogate modeling and solving the issue of negative transfer.
134 In this paper, the overviews of GPR and TL are presented, and the TL-GPRSM is formulated. Then,
135 two case studies are conducted to demonstrate the effectiveness of TL-GPRSM. The first is the live-
136 load performance evaluation analysis of a steel plate girder bridge. Here, the target domain is the
137 maximum stress evaluation of the bridge with corrosion damages, and the source domain is that of
138 the bridge in the initial undamaged condition. The second case study is on the seismic performance
139 evaluation of a seismic isolation bridge pier that requires nonlinear time-history analysis. Here, the
140 target domain is the maximum displacement evaluation of the bridge pier and rubber bearing with
141 the input as the recorded earthquake ground motion, and the source domain contains the inputs of
142 ground motions provided in the design standard. The effectiveness of the TL-GPRSM is verified
143 based on the accuracy of the constructed surrogate models and effect of computational cost
144 reductions. In addition, the contribution of TL is discussed using the similarity evaluation based on
145 ARD. Further, the contributions of uncertain parameters estimated through ARD to the output are
146 validated using structural engineering observations.

2. Transfer training in GPR surrogate modeling

The TL-GPRSM developed in this paper is explained in this section. First, an outline of GPR with the ARD kernel function is presented, and the incorporation of TL into the GPR is demonstrated. In addition, the application of the estimated ARD parameters to validate the constructed TL-GPRSM and effect of TL is explained.

2.1 GPR with ARD kernel

GPR [15] is a nonparametric regression method and applicable to various input–output relationships. First, suppose an input-and-output data matrix **D** with number of data *N* is defined as shown below.

$$\mathbf{D} = \{(\mathbf{x}_1, y_1), (\mathbf{x}_2, y_2), \dots, (\mathbf{x}_N, y_N)\}^T, \tag{1}$$

where **x** is a vector of the input parameters with length of *L*, and *y* is the output. The input–output relationship is described as

$$y = f(\mathbf{x}). \tag{2}$$

Suppose that *y* is standardized to the zero-mean variable, and *f* is supposed to be generated from the following GP with zero mean.

$$f \sim \mathrm{GP}\big(\mathbf{0}, k(\mathbf{x}, \mathbf{x}')\big). \tag{3}$$

Here, GP represents the Gaussian process and *k* is a kernel function used to calculate the kernel matrix **K**, which has *N* rows and *N* columns.

$$K_{nm} = k(\mathbf{x}_n, \mathbf{x}_m), \tag{4}$$

where K_{nm} is the element of **K** with *n* rows and *m* columns. Because *f* in Eq. (2) follows the GP, as shown in Eq. (3), the output vector $\mathbf{y} = (y_1, y_2, \dots, y_N)^T$ also follows the Gaussian distribution with zero mean and covariance matrix **K**.

$$\mathbf{y} \sim \mathcal{N}(\mathbf{0}, \mathbf{K}). \tag{5}$$

In this paper, we used the autoregressive relevance determination (ARD) kernel function [29]. In the ARD, the input parameters that contribute to the output can be determined automatically. Further, the

performance of regression in GPR depends on the selection of the kernel function. For instance, if the Matern5/2 kernel is selected, ARD is applied as

$$k(r,\boldsymbol{\theta}) = \sigma^2\left(1+\sqrt{5}r+\frac{5}{3}r^2\right)\exp(-\sqrt{5}r)\,, \quad \text{where} \quad r(\mathbf{x}_n,\mathbf{x}_m) = \sqrt{\sum_{i=1}^{L}\frac{(x_{ni}-x_{mi})^2}{l_i^2}}. \tag{6}$$

Here, L is the number of dimensions of the input parameter vector, and $\boldsymbol{\theta}$ is a vector of the hyperparameters σ and l_i. Among these hyperparameters, l_i is called the length-scale, which indicates the contribution of the input parameter x_i in the ARD. The smaller the estimation of the length-scale l_i, the larger is the contribution of x_i to the output y. The estimator of GPR with ARD is thus the hyperparameter $\boldsymbol{\theta}$, which includes the length-scale l_i. To verify the contribution of each parameter, index c_i was defined, which was the index converted from the length-scale l_i to the relative percentage contribution in each input dimension i, as below.

$$c_i = \frac{1/l_i}{\sum_{j=1}^{L}(1/l_j)} \times 100 \qquad (i = 1,2,\cdots,L) \tag{7}$$

In this study, the maximum likelihood estimation was used for estimating the hyperparameters of GPR model $\boldsymbol{\theta}$ by adopting the limited-memory Broyden–Fletcher–Goldfarb–Shanno (L-BFGS) method [31] as the optimization method. The GPR model construction was implemented using the Python library GPy [32].

2.2. TL in TL-GPRSM

TL in TL-GPRSM is implemented by the data expansion proposed by Daumé [33]. This method can apply to TL in most machine learning models including GPR by expanding the matrix of input parameters in training data to the common, source, and target parts. This makes possible to implement TL without losing advantages of GPR, applicability to nonlinear and nonparametric regressions. Furthermore, as the ARD kernel can be applied straightforward, the explainability of constructed TL-GPRSM is introduced including the effectiveness of TL.

The input–output relationship of the target numerical analysis for surrogate modeling is called the "target domain." The "source domain" is the input–output relationship of the previously trained model. For successful TL, the input–output relationship of the source domain is required to be similar to that of the target domain. First, suppose that the source domain data $\mathbf{D}^s$ and target domain data $\mathbf{D}^t$ are described as

$$\mathbf{D}^s = \left\{(\mathbf{x}_1^s, y_1^s), (\mathbf{x}_2^s, y_2^s), \ldots, \left(\mathbf{x}_{N_s}^s, y_{N_s}^s\right)\right\}, \tag{8}$$

$$\mathbf{D}^t = \left\{(\mathbf{x}_1^t, y_1^t), (\mathbf{x}_2^t, y_2^t), \ldots, \left(\mathbf{x}_{N_t}^t, y_{N_t}^t\right)\right\}, \tag{9}$$

where the vector $\mathbf{x}$ is the input variables vector and y is output value. The number of data in the source domain is N_s and that in the target domain is N_t. The data expansion for TL is implemented by configuring the expanded input vectors for the target domain $\hat{\mathbf{x}}^t$ and source domain $\hat{\mathbf{x}}^s$ using input vectors $\mathbf{x}^s$ and $\mathbf{x}^t$, respectively, as follows:

$$\hat{\mathbf{x}}^s = (\mathbf{x}^s, \mathbf{x}^s, \mathbf{0}) \quad \text{and} \quad \hat{\mathbf{x}}^t = (\mathbf{x}^t, \mathbf{0}, \mathbf{x}^t). \tag{10}$$

The expanded input and output data $\mathbf{D}^{TL\text{-}GPRSM}$ for TL-GPRSM are as follows:

$$\mathbf{D}^{TL\text{-}GPRSM} = \left\{(\hat{\mathbf{x}}_1^s, y_1^s), (\hat{\mathbf{x}}_2^s, y_2^s), \ldots, \left(\hat{\mathbf{x}}_{N_s}^s, y_{N_s}^s\right), (\hat{\mathbf{x}}_1^t, y_1^t), (\hat{\mathbf{x}}_2^t, y_2^t), \ldots, \left(\hat{\mathbf{x}}_{N_T}^t, y_{N_T}^t\right)\right\}^T. \tag{11}$$

TL can be realized by constructing a GPR model using the data matrix in Eq. (11) as training data. The objective of this formulation is to expand the input vector $\mathbf{x}$ to three parts: "common part," "source part," and "target part," as shown in Fig. 1. TL-GPRSM is then realized by constructing a GPR model using these expanded data. This means that the information of the source domain is used in training the target domain model. Within the expanded input and output data, the common part considers both the source and target domains, the source part considers only the source domain, and the target part considers only the target domain. The contribution of each part to the constructed GPR model indicates the utility of the TL. By adopting the ARD kernel for GPR, it becomes possible to derive the contribution of each part. Here, the contribution of each input dimension can also be derived using Eq. (7). The contribution for each part can be calculated by adding the contribution c_i, where i indicates the component corresponding to each part.

$$C_C = \sum_{i=1}^{L_C} c_i, \quad C_S = \sum_{i=1}^{L_S} c_i, \text{ and } \quad C_T = \sum_{i=1}^{L_T} c_i. \tag{12}$$

Here, C_C, C_S, and C_T are the contributions of the common, source, and target parts, and L_C, L_S, and L_T are the number of input dimensions of the common, source, and target parts, respectively. Considering that the common part contributes to both the source and target domains, the relative magnitude of C_C against C_T indicates the effect of TL in predicting in the target domain.

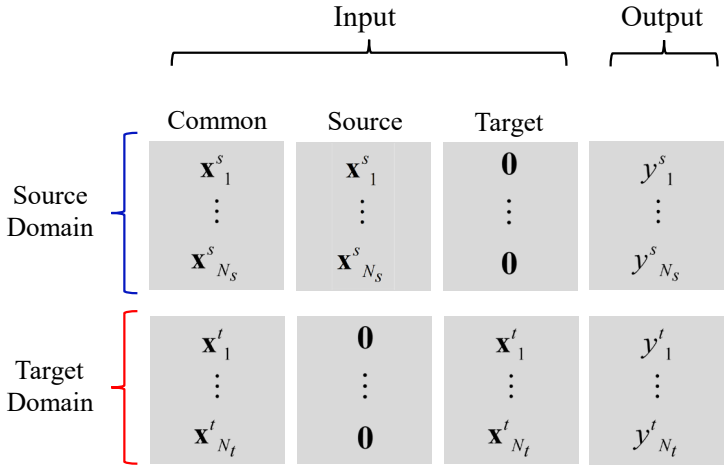

Fig. 1 Data expansion for incorporating TL into GPR

2.3. Construction and validation of TL-GPRSM

In the construction of TL-GPRSM developed in this paper, the training and test datasets for the source and target domains are created through numerical calculations of the structural model with the input parameter sets generated by Latin hypercube sampling (LHS) [34]. The hyperparameters of GPR are then estimated using L-BFGS optimization.

The performance of constructed surrogate model was evaluated by the prediction error with respect to the test data and the accuracy of predicted probability distribution of output, which is required for the structural reliability analysis. It is particularly important for the surrogate modeling for structural reliability analysis to be able to predict the appropriate distribution of output response. The root means square percent error (RMSPE) was used for the evaluation of the prediction error. The

agreement of distributions was evaluated using not only the overlay of cumulative distributions but also the p-value in the Kolmogorov–Smirnov (KS) test. In each verification case, the surrogate model was constructed for the ten training datasets created through ten trials of LHS sampling, and the variations in the accuracy and probability distributions were derived for evaluating the modeling stability.

The computational cost of surrogate modeling was evaluated by the required number of times of numerical calculations of the structural model (e.g., FE model) to predict the accurate distribution of output response. Here, it should be noted that the computational cost of prediction using constructed surrogate model is negligible compared to the computational cost of numerical analysis of the structural model. The TL-GPRSM is expected to realize reducing the number of training data in the target domain by taking advantage of data in the source domain, which has been already existed.

The explainability of the constructed surrogate model and confidence assurance of the TL were then evaluated based on the percentage contributions derived using the estimated length-scales in the ARD kernel. Structural reliability analysis is the procedure of considering the uncertainties of multiple parameters for evaluating the limit state capacity. However, the number of parameters contributing to the output required for the performance evaluation is actually limited in many cases. This sparsity of the contribution can be estimated by using the ARD kernel. The contribution of each input dimension c_i, derived using Eq. (7) with the estimated length-scale l_i, indicates the extent to which the uncertainty of the corresponding model parameter affects the demand output. The constructed surrogate model can be accepted when the contributing model parameters can explain the structural response output behaviors from the viewpoint of the physics of the structure. Furthermore, the contributions of the common, source, and target parts, which are the summed contributions of the dimensions belonging to each part, calculated using Eq. (12), is used for evaluating the effectiveness of TL. Here, TL is considered effective when the contribution of the common part Cc against C_T is relatively high.

263

264 **2.4. Application example of TL-GPRSM**

265 A simple application example is shown to recognize the significance of TL-GPRSM. Here, the
266 function models, f_s and f_t, are given as the source domain and the target domain, respectively.

267 $$f_s(\mathbf{x}) = 2{x_1}^2 + {x_2}^2 + 0.00001x_3 + 5 \tag{13}$$

268 $$f_t(\mathbf{x}) = 2{x_1}^2 - 2\,(x_2 - 1)\sin x_2 + 0.00001x_3 + 5 \tag{14}$$

269 where x_1, x_2, and x_3 are input variables with the range of $-1 \le x_i \le 1$ (i =1−3), and the input vector is
270 configured as $\mathbf{x}=(x_1, x_2, x_3)$. Seeing the similarity between those two function models, only the terms
271 of x_2 acts on the output differences between the models of source domain f_s and target domain f_t, and
272 contributions of the terms of x_1 and x_3 and the constant terms are the same in both models. In
273 addition, the coefficient of each term indicates how much that term contributes to the output of
274 function. It is obvious that coefficients on x_3 are relatively small in both models.

275 First, the data sets of function input-output relationships for source domain f_s and target domain f_t are
276 created with the numbers of data N_s =100 and N_t =10, respectively. The samples of input variables
277 space are plotted in Fig.2, where they are shown in the spaces of x_1 and x_2 because x_3 less contributes
278 to the function output, as mentioned above. The data matrix of source domain $\mathbf{D}^s$ and target domain
279 $\mathbf{D}^t$ are represented as:

280 $$\mathbf{D}^s = \{(\mathbf{x}_1^s, f_s(\mathbf{x}_1^s)), (\mathbf{x}_2^s, f_s(\mathbf{x}_2^s)), \dots, (\mathbf{x}_{100}^s, f_s(\mathbf{x}_{100}^s))\}^T. \tag{15}$$

281 $$\mathbf{D}^t = \{(\mathbf{x}_1^t, f_t(\mathbf{x}_1^t)), (\mathbf{x}_2^t, f_t(\mathbf{x}_2^t)), \dots, (\mathbf{x}_{10}^t, f_t(\mathbf{x}_{10}^t))\}^T, \tag{16}$$

282 Then, the expanded input vectors for implementing TL are configured following Eq. (10), as:

283 $$\hat{\mathbf{x}}^s{}_i = (\mathbf{x}^s{}_i, \mathbf{x}^s{}_i, \mathbf{0}_{\mathbf{1}\times\mathbf{3}})(i = 1 - 100) \quad \text{and} \quad \hat{\mathbf{x}}^t{}_j = (\mathbf{x}^t{}_j, \mathbf{0}_{\mathbf{1}\times\mathbf{3}}, \mathbf{x}^t{}_j)\ (j = 1 - 10). \tag{17}$$

284 The data matrix for TL-GPRSM is given as follows:

285 $$\mathbf{D}^{TL-GPRSM} = \{(\hat{\mathbf{x}}^s{}_1, f_s(\mathbf{x}_1^s)), (\hat{\mathbf{x}}^s{}_2, f_s(\mathbf{x}_2^s)), \dots, (\hat{\mathbf{x}}^s{}_{100}, f_s(\mathbf{x}_{100}^s)), (\hat{\mathbf{x}}^t{}_1, f_t(\mathbf{x}_1^t)), (\hat{\mathbf{x}}^t{}_2\ , f_t(\mathbf{x}_2^t)), \dots, (\hat{\mathbf{x}}^t{}_{10}, f_t(\mathbf{x}_{10}^t))\}^T \tag{18}$$

286 The obtained surrogate model for target domain f_t is then evaluated by predicting the distribution of
287 function outputs to 1000 samples generated from the space of input variables x_i with range of $-1 \le x_i$

288 ≤1 (i =1−3). For comparison, a GPR surrogate model without TL is also constructed only using the
289 10 data from the target function model f_t. The predicted distributions are compared in Fig.3 (a). Here,
290 the distribution of function outputs created by assigning the same 1000 samples of input variables to
291 the target function model f_t is also shown as “True” case. The TL-GPRSM can predict the
292 distribution closer to the true distribution than the one predicted from the GPR model without TL.
293 The RMSPE accuracies are 0.13% and 15.2% in TL-GPRSM and GPR without TL, respectively.
294 Also, the function field of f_t predicted by the TL-GPRSM in Fig. 3(b) clearly shows good agreement
295 with the true function field, which is shown in Fig. 2(b), compared to the function field predicted by
296 the GPR without TL in Fig. 3(c).
297 The contribution of each input variable in each of "Common," "Source," and "Target" parts is then
298 evaluated by calculating c_j using Eq. (7) as:

299 $$c_j = \frac{1/l_j}{\sum_{j=1}^{9}(1/l_j)} \times 100 \qquad (j = 1, \cdots, 9), \tag{19}$$

300 where l_j is length-scale in ARD kernel, and subscript j indicates the order of each input parameter in
301 expansion data, i.e., j=1−3 indicates three input variables x_1-x_3 in “Common” part, j=4−6 indicates
302 those in “Source” part, and j=7−9 are those in “Target” part. Those parts correspond to the
303 “Common”, “Source”, and “Target” parts presented in Fig.1. Figure 4 shows calculated contribution
304 index c_j. In the “Common” part, only input variable x_1 has non-zero value. This indicates that the
305 terms of x_1 contribute similarly to both function outputs of the source domain f_s and the target
306 domain f_t. On the other hand, there is no contribution in x_2 in “Common” part, and the term of x_2
307 shows significant contribution in each of “Source” and “Target” parts. These points are
308 understandable because the terms of x_1 are the same in the two function models, f_s and f_t, and the
309 terms of x_2 are different between them, as shown in Eqs. (13) and (14). In addition, almost zero
310 values in x_3 in all parts indicate consistency with the point that the terms of x_3 have small coefficients
311 in both model functions.

The effect of TL can be determined by the summation of contribution c_j in each part, which are C_C, C_S, and C_T expressed in Eq. (12). The calculated values of C_C, C_S, and C_T are 39.5, 27.1 and 33.4, respectively. It can be said that the TL worked effectively for the appropriate surrogate modeling from the point that the relative value of common part contribution C_C against target part contribution C_T was large in this application example.

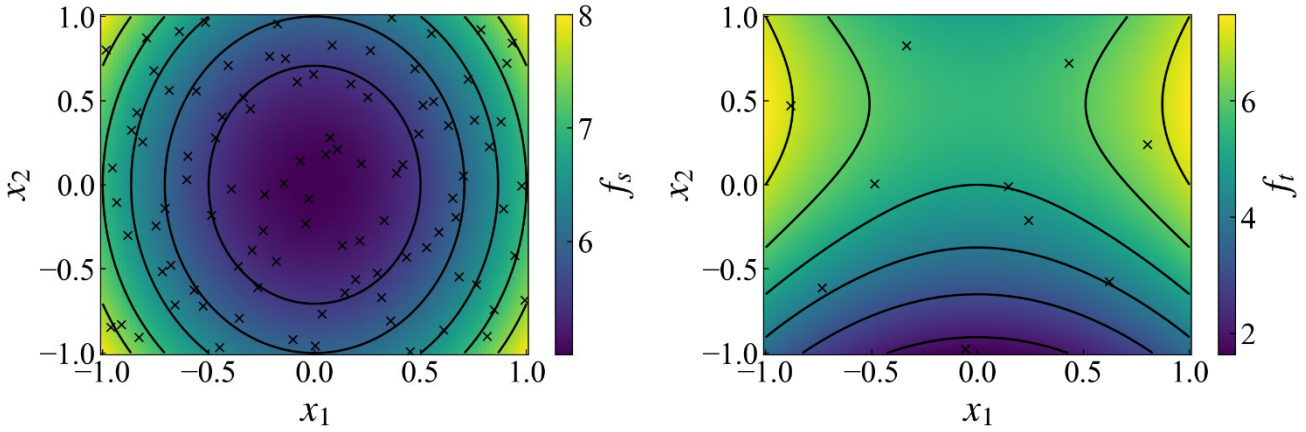

(a) Source domain (data samples N_S=100) (b) Target domain (data samples N_T=10)

Fig. 2 Function field of source and target domain models and created training data (described in "×")

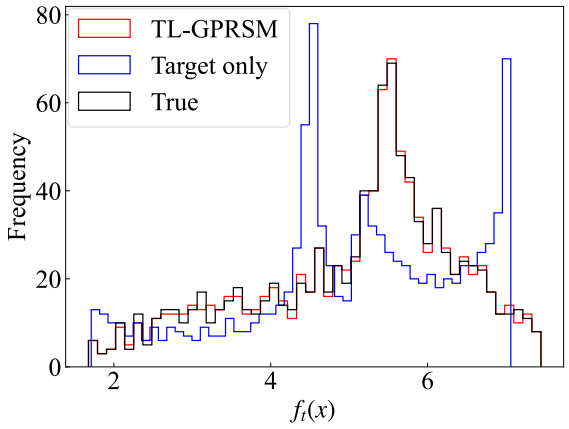

(a) Distributions of function outputs

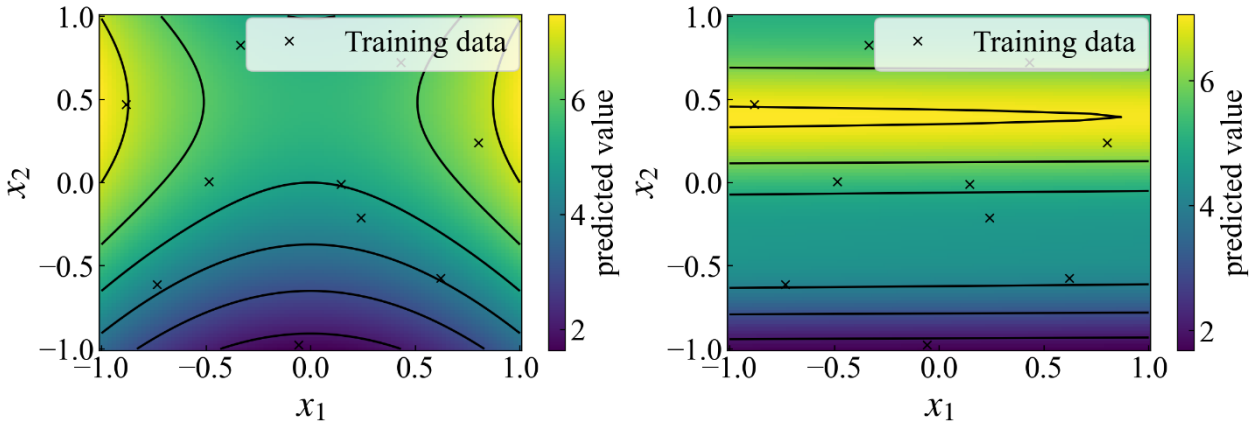

(b) Predicted function field (TL-GPRSM) (c) Predicted function field (GPR without TL)

Fig. 3 Prediction performance of constructed surrogate models for target function model f_t

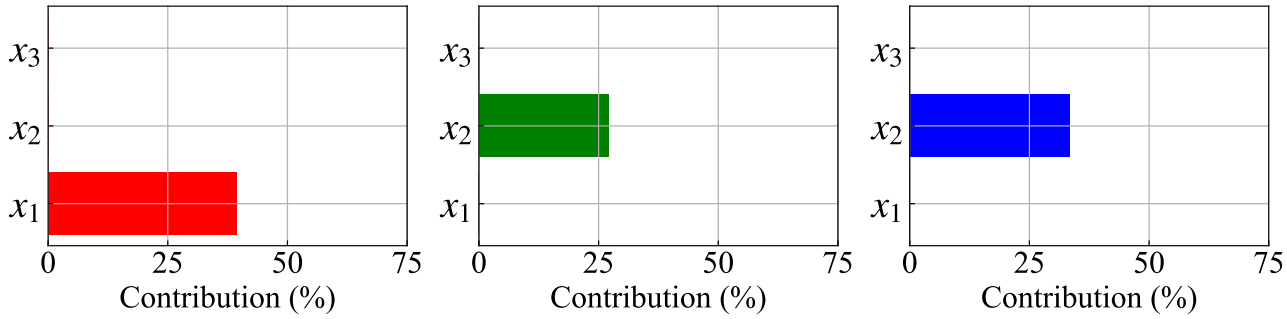

Fig. 4 Estimated contributions of model parameter uncertainties
(Left: Common part, Center: Source part, Right: Target part)

3. Live-load capacity evaluation of plate girder bridge

TL-GPRSM is expected to be applicable to the case wherein the number of input parameters and their uncertainties change in the source and target domains of the TL. In existing structures, the number of uncertain parameters and their degrees of uncertainties may change from those at the time of new construction owing to damage or deterioration. In this case, if TL-GPRSM is effective, the computational cost of the reliability analysis can be reduced by using the data saved in the design phase. In this section, we use the analytical model of a steel plate girder bridge with damaged sections. The surrogate model was constructed by applying TL-GPRSM to the data before and after the damage, and its effectiveness in reducing the computational cost was verified. The effectiveness of TL and adaptation to the sparsity of input parameters using ARD contribution estimation were also

verified.

3.1 FE modeling and evaluation analysis

The numerical analysis as the target of surrogate modeling in this paper was the structural reliability analysis of a simply supported steel plate girder bridge considering the damage of corrosion at the end of the main girder, which was conducted in a previous study by the authors [35]. The bridge is a testbed structure for the numerical study designed based on the Japanese design standard [36]. The bridge consists of five main I-shape steel girders, a reinforced concrete (RC) slab, and steel bearings with a span length of 20.0 m and width of 10.7 m. The FE model of the bridge was constructed using the general-purpose FE analysis software Abaqus 6.14. Figure 5(a) shows the overall view of the constructed whole-bridge FE model. Here, the five main girders and concrete slab were modeled using the shell element, and the members of the steel bearings were described using the solid element. The output response for the performance evaluation was the maximum Mises stress at the region near the ends of each main girder under static loading of the designed live load introduced in the Japanese design standard [36]. The convergence of the mesh size to the output response was verified to determine the mesh size configuration for the whole-bridge model; however, the determined number of elements became excessively large. Therefore, the half-girder model was prepared to reduce the computational cost, as shown in Fig. 5(a). Here, the previously determined mesh configuration was retained, and the continuity condition at the mid-span cross-section was applied with symmetry preservation. In addition, the input live load was adjusted to obtain the stress distribution at the main girder as the output, which was consistent with that obtained in the whole-bridge model analysis. The total number of elements in the half-girder model was 104,799. Most parameters of the initial model without damages were determined based on the nominal properties of steel and RC used in the bridge design. The friction coefficient of the contact surface between the upper and lower parts of the steel bearing was set to 0.2, which is the generally used value of the

coefficient for metal contact surfaces. In the constructed initial FE model, the static deflection under the designed live load satisfied the requirement for the limit state in the design standard [36]. Then, the FE model for the performance evaluation under the damaged condition was constructed. The corrosion at the main girders and bearings was represented by setting the individual areas in the main girders, as shown in Fig. 5(b), to reduce the thickness at the corroded areas and by increasing the friction coefficients at the corroded bearings, respectively. The effect of cracks at the concrete slab was considered by reducing the Young's modulus of the elements of the slab. The input–output relationship of the initial FE model is the source domain, and that of the FE model with damages is the target domain in the TL-GPRSM.

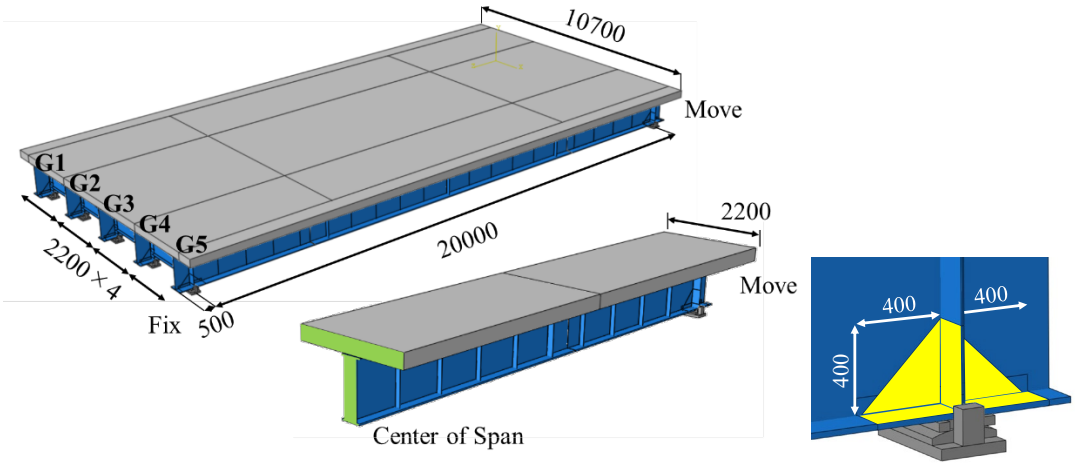

(a) Full bridge model and its half-girder model (b) Corroded area

Fig. 5 Testbed bridge FE model for verification

3.2 Uncertainties of model parameters

In the TL-GPRSM, the increase in the uncertainties in the structural properties due to damages is considered through TL. The parameter uncertainties were determined both in the initial FE model as the source model and in the damaged-condition FE model as the target model. In the initial FE model, sixteen parameters #1–#16 were considered, and their uncertainties were represented by the uniform distributions with nominal mean and coefficient of variation (COV), as shown in Table 1. Here, the mean and COV values were determined based on the statistical properties reported in previous

research papers and surveys, as summarized in the authors' previous study [35]. For the damaged-condition FE model, three parameters #17–#19 were added to represent the effect of corrosion, that is, the thickness reduction at the corroded areas. In addition, the probability distribution of the friction coefficient #8 (C_f) was changed to represent the decrease in the moving function due to the corrosion, and the distribution of the Young's modulus of the concrete slab #3 (E_c) was changed to consider the effect of cracks.

Figure 6 shows the distributions of the maximum Mises stress near the ends of the girders for the performance evaluation using MC calculations with 500 samples from the space of uncertain model parameters in the initial- and damaged-condition FE models. Here, the 500 samples were generated through LHS. The maximum Mises stress in the damaged-condition FE model is distributed in the range of higher stress values when compared with the distribution in the initial FE model. It can be said that the limit state capacity of yield stress is reduced owing to the damages. The distribution of the maximum Mises stress in the damaged-condition FE model is the target output of the surrogate modeling using the TL-GPRSM. The surrogate model for the initial FE model with sixteen uncertain model parameters as the inputs is the source domain, and that for the damaged-condition FE model with nineteen parameters as the inputs is the target domain. Although the number of input parameters is different between the source and target domains, the TL-GPRSM is applied by data expansion with 16 dimensions for the common part, 16 dimensions for the source part, and 19 dimensions for the target part.

410

411 Table 1 Uncertainties of FE model parameters (−: N/A, *: the same as in the initial FE model)

	FE model parameter (Unit)		Initial (Source)		Damaged (Target)	
			Nominal	COV	Nominal	COV
#1	D_c	Density of concrete slab (kg/m^3)	2400	0.0171	*	*
#2	E_s	Young's modulus of steel main girders (GPa)	200	0.0450	*	*
#3	E_c	Young's modulus of concrete slab (GPa)	25	0.0167	22.5	0.0333
#4	E_b	Young's modulus of steel bearings (GPa)	200	0.0450	*	*
#5	V_s	Poisson's ratio of steel main girder	0.3	0.0910	*	*
#6	V_c	Poisson's ratio of concrete slab	0.2	0.0167	*	*
#7	V_b	Poisson's ratio of steel bearing	0.3	0.0910	*	*
#8	C_f	Friction coefficient of steel bearing	0.2	0.0167	0.9	0.0333
#9	T_{uf1}	Thickness of upper flange of steel girder at near-end section (m)	0.0190	0.0121	*	*
#10	T_{uf2}	Thickness of upper flange of steel girder at mid-span section (m)	0.0300	0.0121	*	*
#11	T_w	Thickness of web plate of steel girder (m)	0.0090	0.0121	*	*
#12	T_{bf1}	Thickness of lower flange of steel girder at near-end section (m)	0.0270	0.0121	*	*
#13	T_{bf2}	Thickness of lower flange of steel girder at mid-span section (m)	0.0300	0.0121	*	*
#14	T_{stc}	Thickness of stiffener of steel girder at near-end section (m)	0.0130	0.0121	*	*
#15	T_{stm}	Thickness of stiffener of steel girder at mid-span section (m)	0.0100	0.0121	*	*
#16	T_{stn}	Thickness of stiffener of steel girder at other sections (m)	0.0065	0.0121	*	*
#17	$T_{bf\text{-}d}$	Thickness of corroded area in lower flange of steel girder at near-end section (m)	–	–	0.025	0.0270
#18	$T_{w\text{-}d}$	Thickness of corroded area in web plate of steel girder (m)	–	–	0.008	0.0162
#19	$T_{st\text{-}d}$	Thickness of corroded area in stiffener of steel girder at near-end section (m)	–	–	0.012	0.0162

412

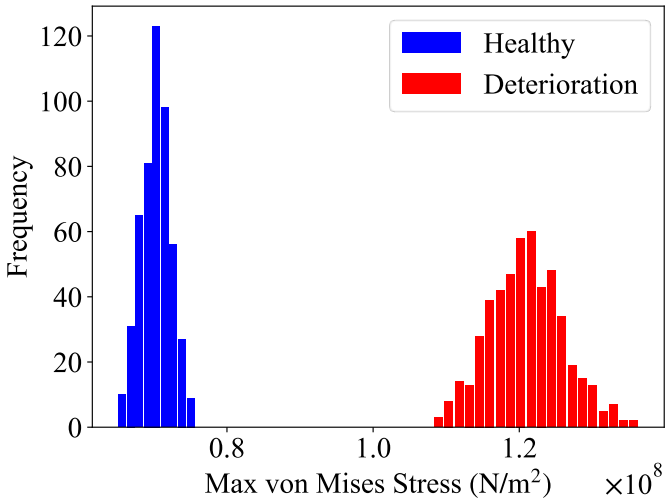

Fig. 6 Distributions of maximum von Mises stress in the steel girder, derived using Monte Carlo calculation of FE models

3.3 TL for FE model analysis in damaged condition

The training dataset in the source domain was configured using the sampled 16-dimension uncertain model parameter sets and their output responses, i.e., the maximum Mises stress near the end of the girder, in the initial FE model. The dataset in the target domain comprised the inputs sampled from the space of 19-dimension uncertain parameters and their output responses in the damaged-condition FE model. The TL-GPRSM was constructed using the input-output data from the FE analysis in the initial condition as the source domain and the input-output data from the FE analysis in the damaged condition as the target domain.

In the verification, a fundamental dataset that consists of 500 input–output relationships was prepared by conducting FE analysis for 500 input model parameter samples to configure the training and test datasets in the target domain. For N number of training data, N input–output relationships were randomly selected from the fundamental dataset, and the remaining were used as the test data. The accuracy of the surrogate model was verified using the RMSPE. The p-value of the KS test was also derived to evaluate the agreement between the maximum Mises stress distributions from the surrogate model and those from the MC calculation using the FE model. In each case, surrogate modeling was performed for ten training datasets for evaluating the modeling stability.

The number of training data in the source domain, i.e., the initial FE model, was varied to evaluate how it affected the accuracy of the TL-GPRSM by setting the cases of 10, 30, and 100 source domain data. The average of RMSPEs for ten GPR surrogate models for the initial FE model in each case was 3.1 in the case of 10 data, 0.10 for 30 data, and 0.0096 for 100 data. It is known that the accuracy of regression increases with the amount of data. The target surrogate model constructed using the TL-GPRSM was then verified. The RMSPE of the constructed surrogate model for the damaged-condition FE model is shown in Fig. 7. Here, the horizontal axis is the number of training data in the target domain. The red line is the accuracy obtained by the TL-GPRSM, and blue line is the result obtained using only the data from the damaged-state FE model. The average and variance of ten surrogate models constructed by ten times samplings were plotted. For each number of source domain data, the RMSPE in the TL-GPRSM converged to a low value faster than that of the surrogate model constructed using only the data from the damage-condition FE model. This indicates that the use of TL-GPRSM can reduce the number of numerical calculations of the damage-condition FE model if there are numerical results from the initial FE model. As the number of source data increases, the RMSPE value and its variation become smaller, i.e., the accuracy and stability of surrogate modeling improve. For all numbers of source domain training data, a surrogate model with accuracy of less than 1% can be obtained by using 15 training data in the target domain. For instance, considering the total computational cost, the accuracy of the surrogate model with 1% RMSPE can be achieved by using 10 source data and 15 target domain data in the TL-GPRSM. Although this accuracy can be obtained by the target-only surrogate model using 25 training data from the damaged-condition FE model, TL-GPRSM ensures higher stability.

The distributions of the maximum Mises stress derived from the constructed surrogate models are depicted in Fig. 8(a). The red lines denote the cumulative distributions of the maximum Mises stress predicted from the surrogate models constructed by the TL-GPRSM using 30 source data and 15 target data. The distributions obtained by ten TL-GPRSMs show good agreement with the

458 distribution obtained by the MC calculation of the FE model, which is shown as a black solid line.
459 The blue lines are the distributions derived through GPR using only the 15 target domain data, which
460 do not agree with the distribution obtained with the FE model MC calculation. Hence, the prediction
461 stability of TL-GPRSM is much higher than that in the case of GPR modeling using only 15 target
462 domain data. In addition, the average of R^2 index, which is to evaluate regression performance, over
463 ten trials, was 0.98 in TL-GPRSM; on the other hand, that in GPR surrogate model without TL was
464 0.57. The R^2 index also indicates that the TL-GPRSM realized more accurate surrogate modeling.
465 The plots of the p-values in the KS test are also shown in Fig. 8(b). The high p-value indicates that
466 the similarity between the two distributions corresponding to the surrogate model and FE model is
467 high. As the number of target domain training data increases, the p-value in the TL-GPRSM reaches
468 a high value faster than that in the case of the GPR model using only the target domain data. It can be
469 concluded that high accuracy and high stability can be obtained using the surrogate model
470 constructed with the TL-GPRSM.
471 Figure 9 shows plots of C_C, C_S, and C_T expressed in Eq. (12) against the number of target domain
472 training data to evaluate the effect of TL. In each plot, the red line shows the relative value of the
473 length-scale sum of the common part, and the blue and green lines show those of the target part and
474 source part, respectively. Each plot represents the ten-time average for each number of target data. In
475 these plots, the higher the value of the common part when compared with that of the target part, the
476 greater is the effect of the TL. In Fig. 9 (a)-(c), the contribution values of all parts are almost
477 converged for the number of target domain data of 10–15 in all cases of the source domain data.
478 Moreover, the effect of TL increases as the number of source domain data increases. The significance
479 of TL is enhanced when a larger number of training data is used in the source domain.
480 Figure 10 shows the contribution of each uncertain model parameter in the constructed surrogate
481 model, that is, the relative value of the inverse length-scale estimated in the TL-GPRSM with 30
482 source domain data and 15 target domain data. The results are shown separately for the expanded

data vector's common, source, and target parts. First, the friction coefficient at the bearings, C_f, shows the highest contribution in the common part. This is interpreted as the similarity in the contribution of parameter C_f to the output in the target and source domains. It can also be seen that the contributions of these parameters are sparse, i.e., some parameters show little contribution; therefore, the significant parameters in the input–output relationship of the target surrogate model can be extracted from this figure. In the initial state analysis of the source domain, the parameters contributed significantly to the overall bending behavior. Regarding parameters with high contributions, the contribution of the steel girder web thickness T_w, which is related to the overall bending stiffness of the girder, was significant. The parameters T_{bf1}, T_{stc}, and E_b representing the characteristics near the girder ends, which are correlated with the boundary conditions, also had an effect. This result is reasonable based on structural engineering findings. However, in the source domain, which is the damaged-state analysis, the contribution was large for parameters related to localized deterioration damage, such as lower flange thickness $T_{bf\text{-}d}$ and web thickness $T_{w\text{-}d}$ at the girder end corrosion area. These estimated contributions are consistent with the findings in structural engineering that the stress at the girder end increases as the corrosion loss progresses. The validity of these estimated contributions supports the explanatory power of the TL-GPRSM.

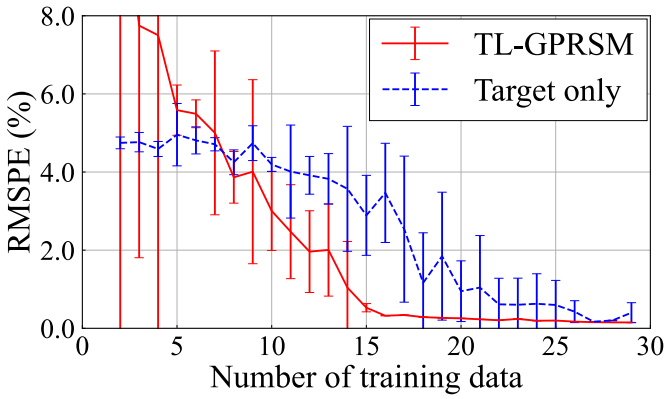

(a) Source domain data: 10

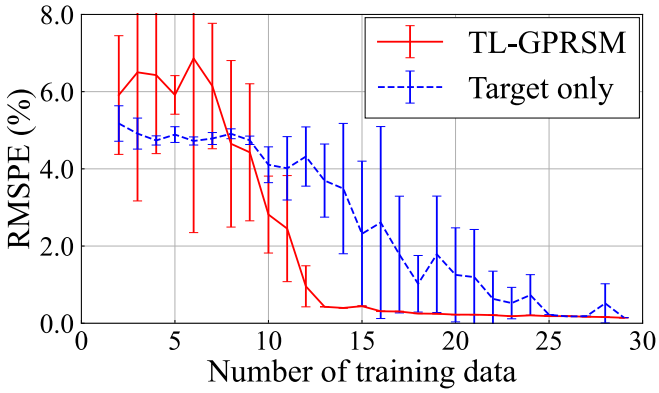

(b) Source domain data: 30

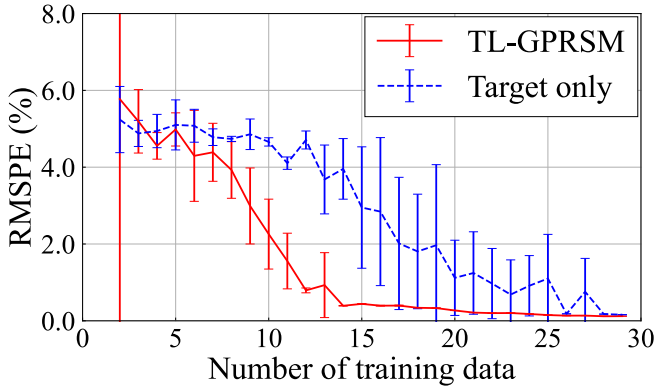

(c) Source domain data: 100

Fig. 7 Accuracy and stability of surrogate model against the number of target domain data

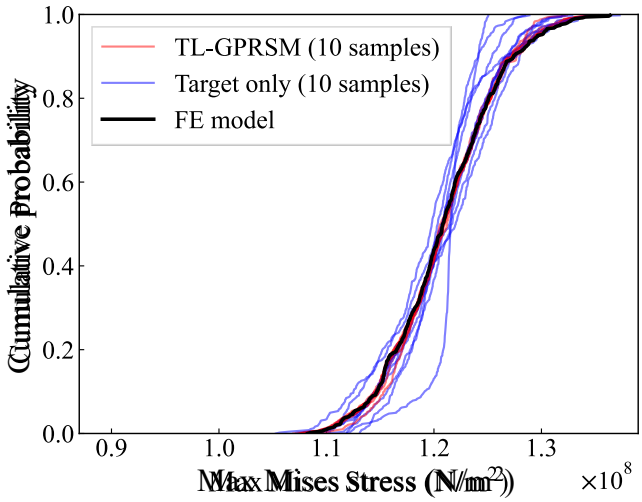

(a) Comparison of cumulative distributions (TL-GPRSM: 30 source domain data and 15 target domain data, Target only: 15 target domain data)

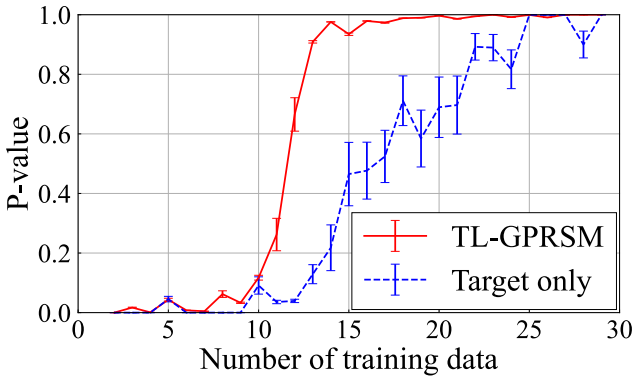

(b) Plot of p-values in KS test (Source domain data: 30)

Fig. 8 Agreement of predicted maximum Mises stress distributions

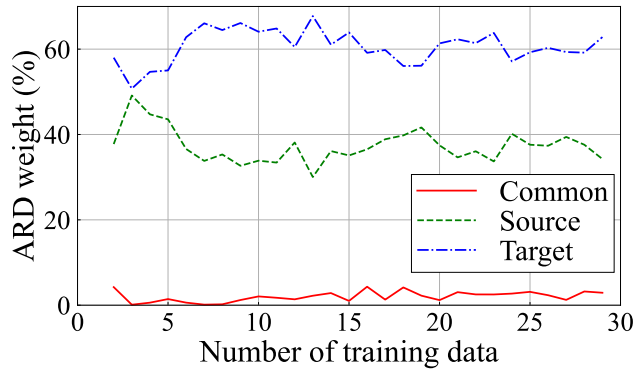

(a) Source domain data: 10

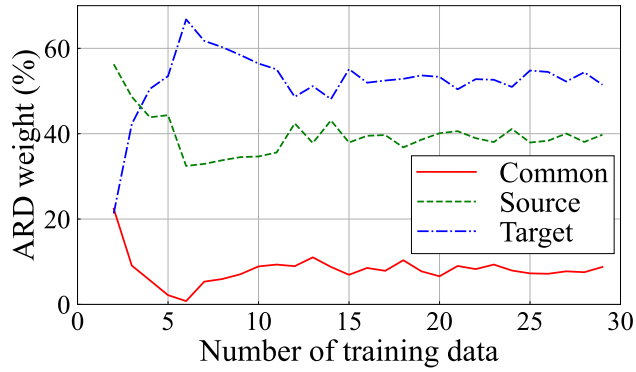

(b) Source domain data: 30

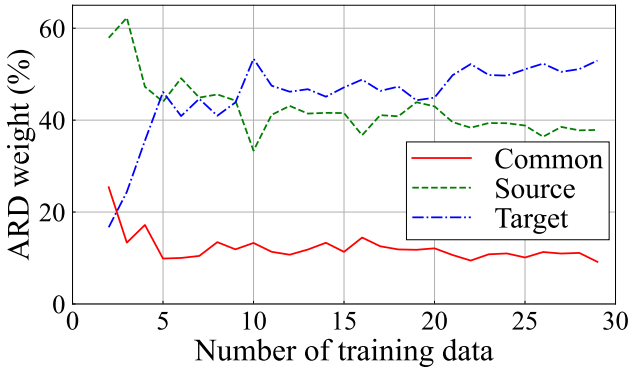

(c) Source domain data: 100

Fig. 9 Contributions of common, target, and source parts in TL

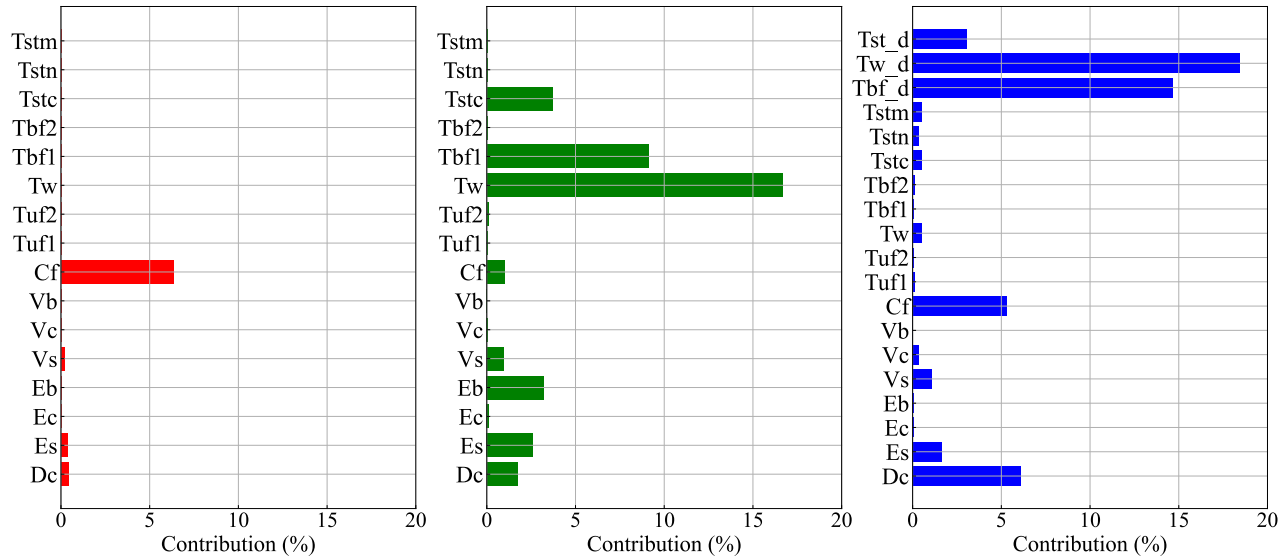

Fig. 10 Estimated contributions of model parameter uncertainties to the maximum Mises stress in the steel girder (number of source data: 30, number of target data: 15) (Left: Common part, Center: Source part, Right: Target part)

4. Performance evaluation of seismic isolated bridge pier

Another application of the structural reliability analysis is performance evaluation against disaster loads such as earthquakes. Here, the structural response analysis requires a nonlinear calculation, and must be performed for various external loads that are probabilistically determined. In this section, the TL-GPRSM was verified using the earthquake response analysis for the seismic performance evaluation of an isolated RC bridge pier. In this section, TL-GPRSM is constructed with the source

domain as the input–output of seismic response analysis with the designed earthquake loads, and the target domain as the input–output of seismic response analysis for a certain input observed earthquake load. We verified whether the computational cost of the seismic performance analysis of the structure could be reduced by using the prepared data created based on numerical analysis with the designed earthquake loads.

4.1 Modeling and parameter uncertainties

The numerical model of a seismic isolation RC pier used in this verification corresponds to the dynamic seismic design shown in the design standard of road bridges in Japan [37]. Figure 11(a) shows the overall view of the bridge, and the target is an RC pier with seismic rubber bearing, indicated as P1. This pier was modeled using the two degree-of-freedom (DOF) lumped-mass model shown in Fig. 11(b). The masses of the superstructure and RC pier were assigned to the upper and lower lumped-masses of the 2DOF system, respectively, and the seismic isolation rubber bearing was modeled as a horizontal spring with nonlinear characteristics described using the bilinear model. The nonlinear stiffness of the RC pier was described using the Takeda model [38]. The nominal parameters were determined based on the values of the bridge properties introduced in the design standard [37], as shown in Table 2. The uncertainty of each model parameter was represented as a uniform distribution with upper and lower limits of ±10% from the nominal value.

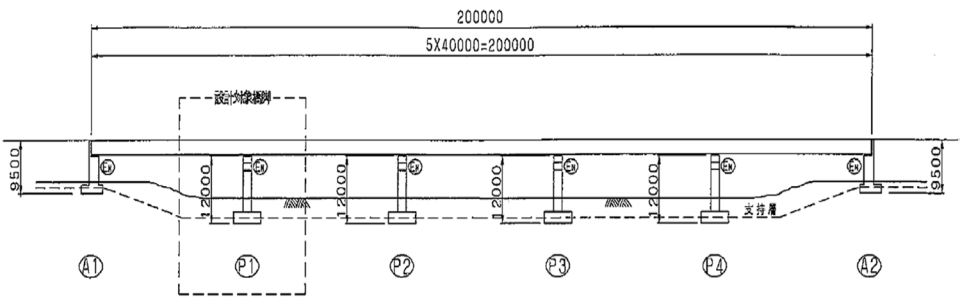

(a) Overall view of the target bridge [37]

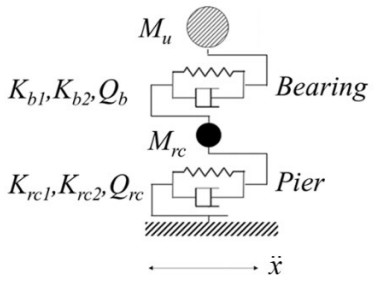

(b) 2DOF lumped-mass model of an isolated RC pier

Fig. 11 Illustrations of target structure

4.2 Input earthquake loads and nonlinear time-history analysis

The input earthquake loads for the target domain in the TL-GPRSM were the designed ground motion in the design standard [39] and two observed earthquake ground motions recorded as JMA Kobe for the Kobe earthquake in 1995 and KAIHOKUBASHI for the Tohoku earthquake in 2011, as shown in Table 3. As the source domain, the designed earthquake ground motion, called Level-2 ground motion, was adopted, which was used for evaluation based on the time-history analysis. Two types of Level-2 ground motions were considered, namely, Type-1 for the plate boundary type earthquake and Type-2 for the inland earthquake. In the design standard [39], three ground motions were prepared for each of Type-1, Type-2, and three ground classifications. Here, the seismic isolation bridge was allowed to be constructed on hard ground; hence, the earthquake ground motions for the corresponding ground classification were used: Type1-1-1/2/3 and Type2-1-1/2/3. For the source domain in all cases, the first ground motions of the two types, Type1-1-1 and Type2-1-1, were adopted. As shown in Table 3, the second ground motion of Type-2, Type2-1-2, was set for the target domain in Case #1. One of the purposes of this verification was to investigate how the similarity in the input earthquake ground motion affected the performance of the TL-GPRSM. It should be noted that JMA KOBE was classified as an inland earthquake (Type-2) and KAIHOKUBASHI as a plate boundary type earthquake (Type-1). The acceleration response spectra for all ground motions for the target and source domains are shown in Fig. 12. In Type-1 ground

583 motion, high response was observed in the low-range period of less than 0.3 s, and the dominant
584 period in Type-2 ranged from approximately 0.3 to 0.8 s. For the nonlinear time-history analysis, the
585 time increment was set to 0.001 s, and the Newmark-β method ($\gamma = 0.5$ m, $\beta = 0.25$) was adopted for
586 the numerical integration. The structural damping was assumed to be Rayleigh damping with the
587 component damping coefficient of 0% for the seismic isolation bearing and 2% for the RC pier.
588 Figure 13(a) and (b) show the response hysteresis of the RC pier and seismic rubber bearing obtained
589 from the results of the time-history analysis for the input cases of JMA KOBE and
590 KAIHOKUBASHI, respectively. Although both earthquake inputs had the same intensity level as the
591 designed input earthquake for each earthquake type, and both showed the maximum displacements in
592 the pier and bearing, the occurrences of nonlinearity were different. In Fig. 13 (a) for JMA KOBE,
593 not only the rubber bearing but also the RC pier showed plasticized responses. However, the RC pier
594 response was in the elastic range by utilizing the rubber bearing in Fig. 13(b) corresponding to
595 KAIHOKUBASHI. It is well known that the nonlinear response of each member strongly depends
596 on the input ground motion. The TL is expected to effectively consider the input–output relationship
597 of each earthquake type trained in the source domain, in the target domain training.
598
599 Table 2 Uncertain parameters of the seismic isolation bridge pier model

Parameter		**Nominal**	**Uncertainty**
Superstructure	Mass (Mu)	604000 kg	± 10 %
Seismic isolation bearing	Primary stiffness (Kb1)	40023.2 kN/m	
	Secondary stiffness (Kb2)	6154.4 kN/m	
	Yield load (Qb)	1117.2 kN	
RC Pier	Mass (Mrc)	346300 kg	
	Primary stiffness (Krc1)	110000 kN/m	
	Secondary stiffness (Krc2)	8250 kN/m	
	Yield load (Qrc)	3399 kN	

600

601

602 Table 3 Target and source domain settings for verification

Case #	Target domain	Source domain
Case #1	Level2 Type2-1-2	Level2 Type1-1-1 (200 data) Level2 Type2-1-1 (200 data)
Case #2	JMA KOBE (Type-2)	Level2 Type1-1-1 (200 data) Level2 Type2-1-1 (200 data)
Case #3	KAIHOKUBASHI (Type-1)	Level2 Type1-1-1 (200 data) Level2 Type2-1-1 (200 data)

603

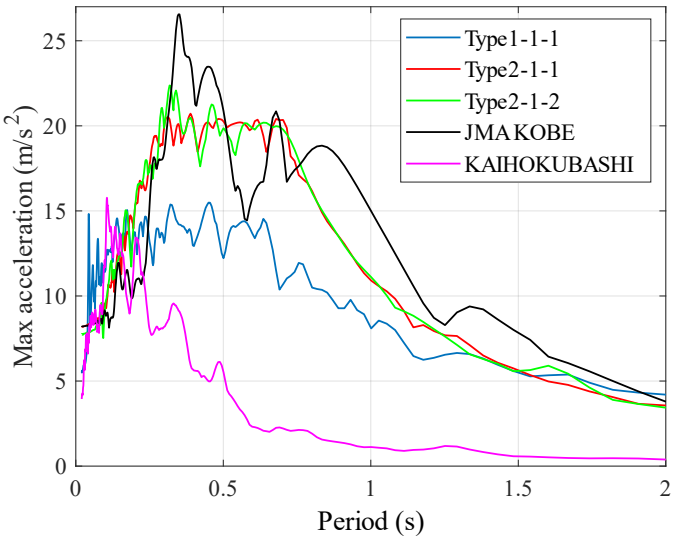

604

605 Fig. 12 Response spectra of earthquake ground motions

606

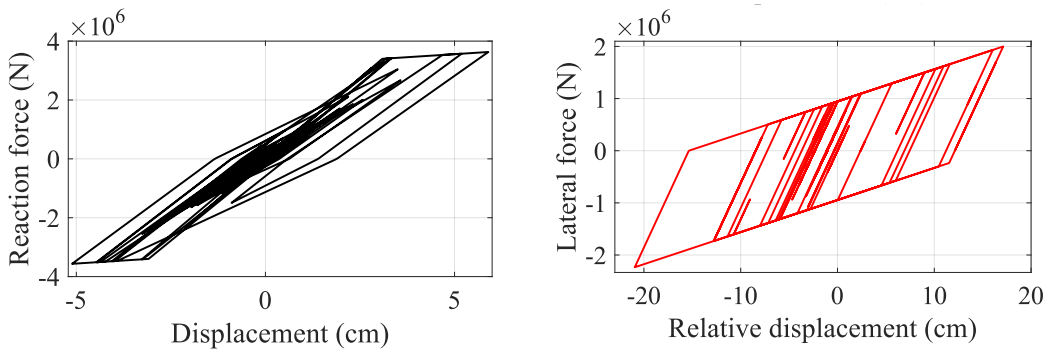

607

608 (a) JMA KOBE (left: pier, right: bearing)

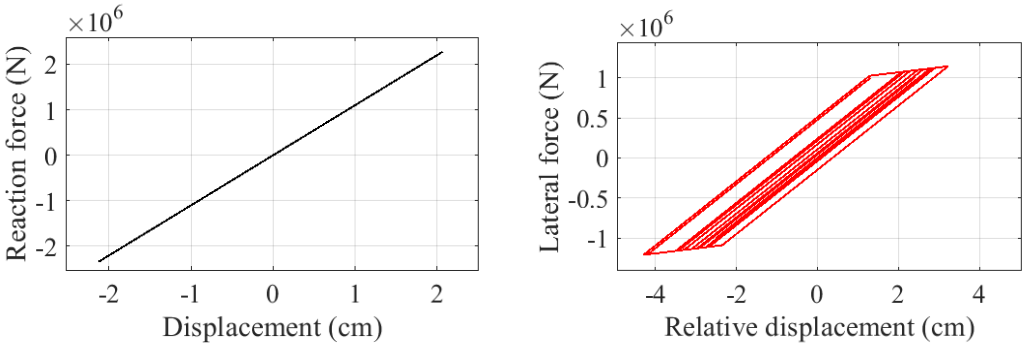

(b) KAIHOKUBASHI (left: pier, right: bearing)

Fig. 13 Response hysteresis with input earthquake ground motions in target domain in Cases #2 and #3

4.3 Surrogate model construction using TL-GPRSM

Figures 14−16 show the accuracies and effects of TL in the constructed surrogate models in Cases #1−#3. In this verification, all surrogate models were constructed using 200 Type1-1-1 data and 200 Type2-1-1 data, with the data having a higher TL effect as the source domain data, as shown in Table 3. For setting the training and testing datasets in the target domain, a fundamental dataset was prepared by creating 10,000 input–output relationships of the nonlinear time-history analysis of the 2DOF lumped-mass model. In each figure, plot (a) depicts the comparison of the accuracies based on RMSPE between the surrogate models constructed using the TL-GPRSM and those constructed using GPR with only the target domain data, plotted against the number of target domain training data. Plot (b) shows the relative contributions of the common, source, and target parts, calculated from the estimated length-scales of ARD, and plot (c) depicts the comparison of the contributions of the common part for each of the two source domains: Type1-1-1 and Type2-1-1.

In Case #1 with the target domain of Type2-1-2, the RMSPE of the TL-GPRSM is slightly lower than that of the surrogate model constructed using GPR in the range of number of target domain data smaller than 50; further, the accuracies in the cases with number of training data over 50 show little difference, as shown in Fig. 14(a). This means that the TL was not useful in ensuring effective surrogate modeling. From the plots in Fig. 14(b), the contribution of the common part to the target

631 part was almost constant, ranging from 10 to 15%, beyond the number of training data of 10. Figure
632 14(c) shows that the contribution of Type2-1-1 was higher than that of Type1-1-1. This means that
633 the output of the maximum displacement of the RC pier mainly considers the source domain of
634 Type2-1-1, which is the same type of input ground motion as that of the target domain. However, the
635 output of the rubber bearing mainly considers Type1-1-1.
636 In Case #2 with the target domain of JMA KOBE, the surrogate models by TL-GPRSM show
637 slightly higher accuracy for both the RC pier and isolation bearing, especially when approximately
638 30 target domain data are used, as shown in Fig. 15(a). Figure 15(b) shows that the relationship
639 between the contributions of the common and target parts is constant, as seen in Case #1, and the
640 ratios of those two contributions are similar. In Fig. 15(c), the contribution of the common part for
641 each of the two source domains shows the same trend as that in Fig. 15(c), both for the RC pier and
642 seismic isolation bearing; however, the difference between the contributions of Type1-1-1 and
643 Type2-1-1 decreases.
644 In the case of KAIHOKUBASHI in Fig. 16(a), the accuracy of the TL-GPRSM for the RC pier
645 almost overlaps that of the surrogate model constructed using only the target domain training data.
646 However, the accuracy of the TL-GPRSM for the bearing improves, especially when the number of
647 training data is less than 100. Considering the range in Fig. 16(b), the contribution of the common
648 part to the target part is relatively high. This indicates that the TL was effective in the surrogate
649 model construction for the RC pier in this case. However, the RMSPE of the bearing surrogate model
650 was approximately three times higher than those of all the other surrogate models, including those of
651 the two previous cases. Figure 16(c) does not show a clear trend in which source domain data were
652 selected in the TL for the surrogate model of the RC pier; however, for the bearing, there was a
653 tendency to select the source domain of Type2-1-1, although the KAIHOKUBASHI ground motion
654 is related to the plate boundary.
655 Figure 17 shows the estimated contributions of each model parameter uncertainty to the demand

output for discussing the explainability of the constructed surrogate models. Here, the contributions to the maximum displacement of the RC pier are shown in Case #2 and Case #3 in Fig. 17(a) and (b), respectively. Notice that highly nonlinear behavior occurred in Case #2 (JMA KOBE) but did not occur in Case #3 (KAIHOKUBASHI), as explained in Fig. 13. The plot of red bars shows the contributions of the model parameters in the common part, the one with green bars denotes those in the source part, and the plot of blue bars denotes the contributions in the target part. It can be first understood that no parameter significantly contributed to the output in the common part in both cases. This is considered the reason why the TL was not effective in these cases. The plot of the target part indicates how each model parameter is considered in each target surrogate model. It can be seen that the contributions of the parameters that are related to the nonlinear behavior, such as *Kb2*, *Qb*, and *Qrc*, are high in Case #2 (JRA KOBE), whereas the contribution of those parameters is much lower in Case #3 (KAHOKUBASHI). These show the consistencies in the structural responses, i.e., occurrences of nonlinearity, which depend on the input earthquake waveform. Even though the effect of TL in computational cost reduction was not achieved by the TL-GPRSM in the cases considered here, the validity of the constructed surrogate models could be assured by observing the estimated contributions. Further considerations of the surrogate modeling of nonlinear dynamic systems with effective TL are required in a future study.

However, the constructed surrogate models can provide appropriate distributions of the maximum displacements for seismic evaluation. Figure 18 shows the cumulative distributions of the maximum displacements of the RC pier and seismic isolation rubber bearing in Case #2. The surrogate model was constructed using TL-GPRSM with the number of target domain data as 50. Ten red lines denote the distributions from the ten surrogate models constructed by ten-time DoE samplings of the data. The black line denotes the distributions derived using the 2DOF model MC calculations with 10,000 samples. Especially in the RC pier, the distribution from the surrogate model shows good agreement with those from the MC calculation along with high stability. In the bearing, the both-side tails of the

distributions from the surrogate models do not show high accuracy and stability.

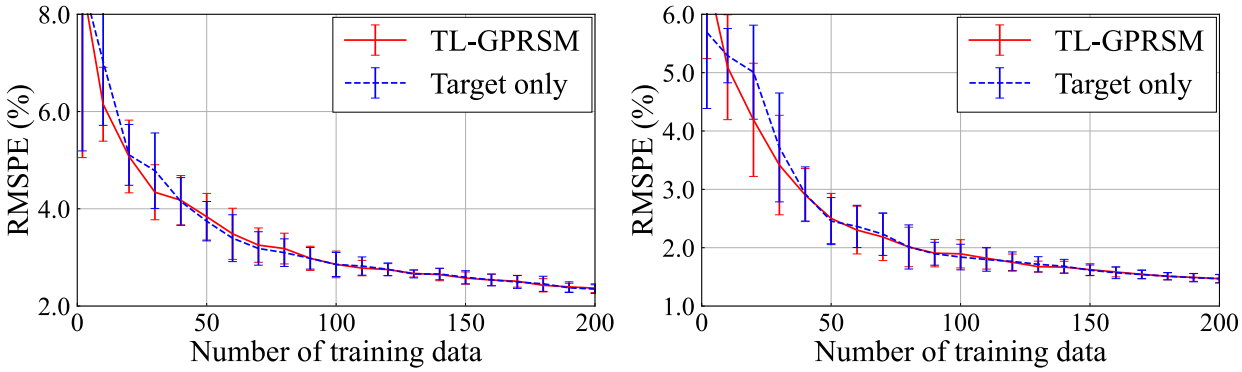

(a) Accuracies of constructed surrogate models (left: pier, right: bearing)

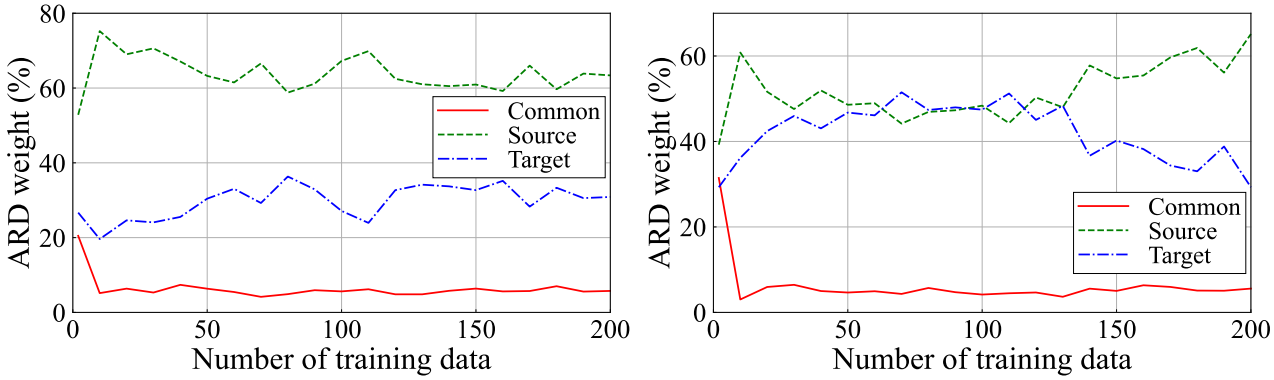

(b) Contributions of common, source, and target domains (left: pier, right: bearing)

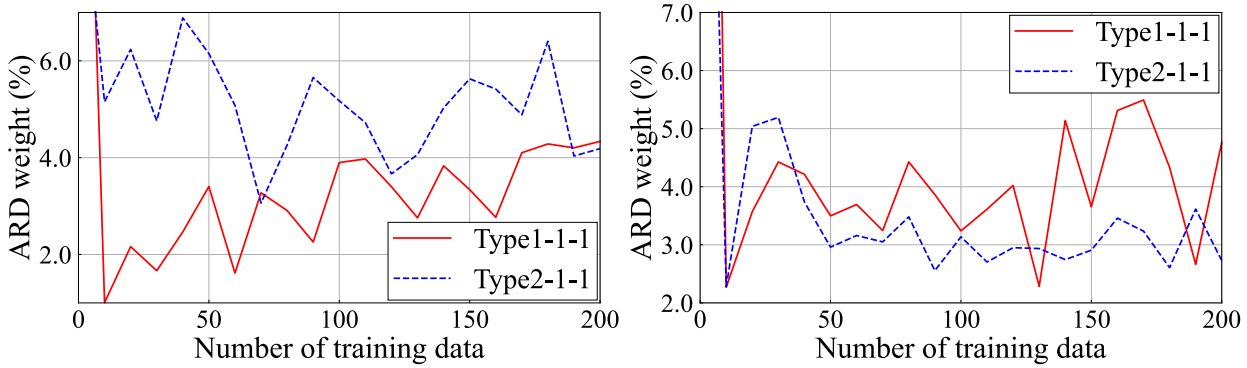

(c) Contribution of common part for each source domain (left: pier, right: bearing)

Fig. 14 Results of surrogate model construction in target domain of Type2-1-2 (Case #1)

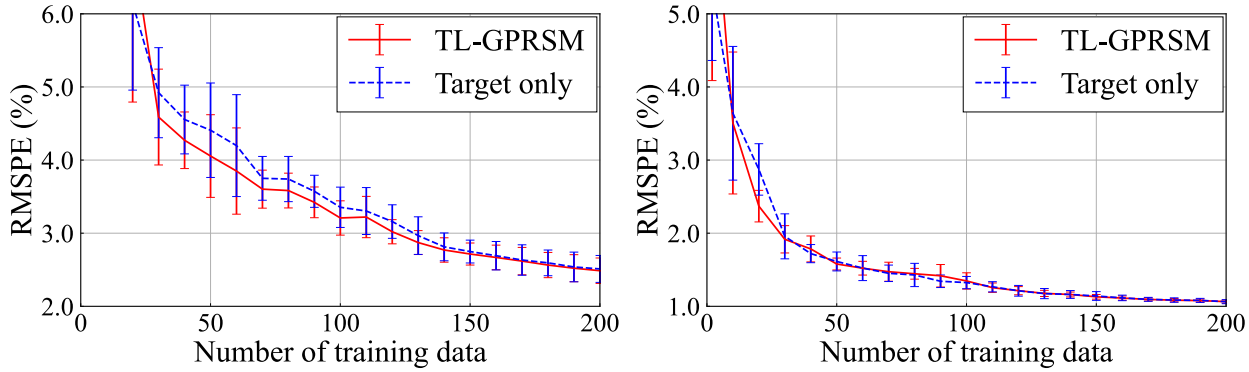

(a) Accuracies of constructed surrogate models (left: pier, right: bearing)

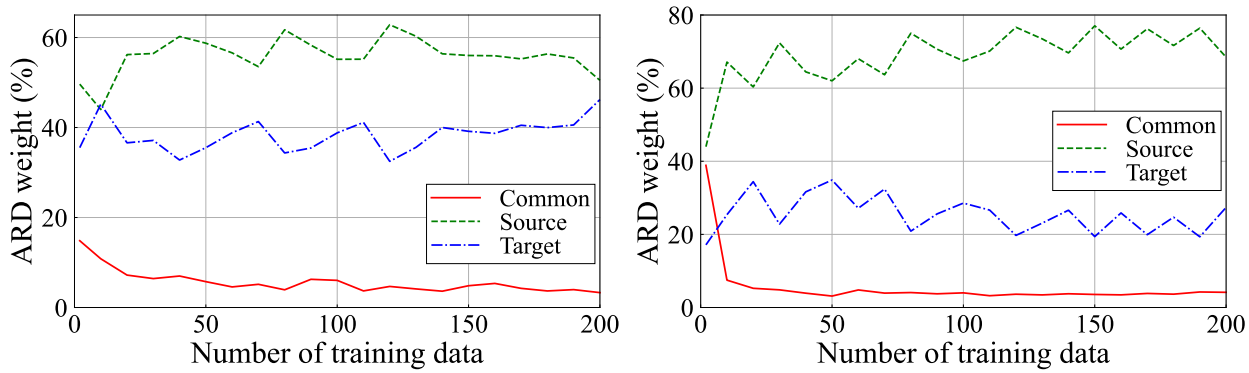

(b) Contributions of common, source, and target domains (left: pier, right: bearing)

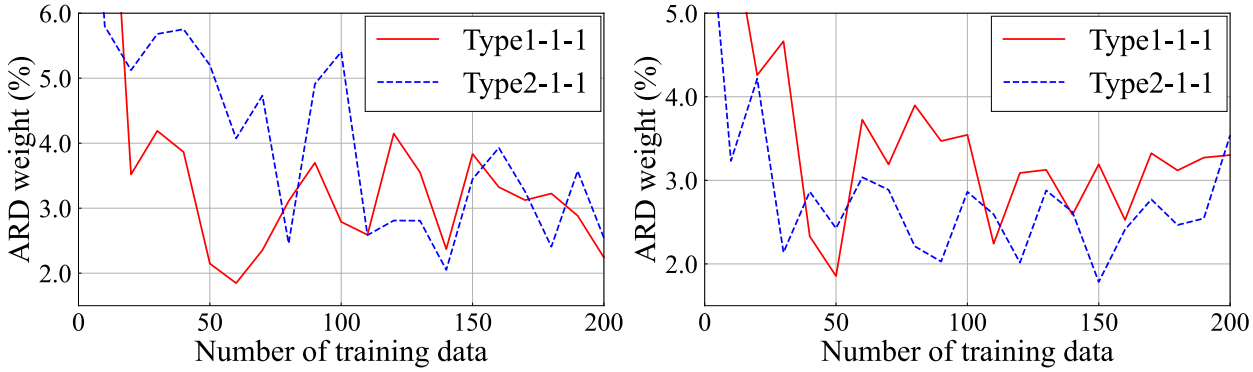

(c) Contribution of common part for each source domain (left: pier, right: bearing)

Fig. 15 Results of surrogate model construction in target domain of JMA KOBE (Case #2)

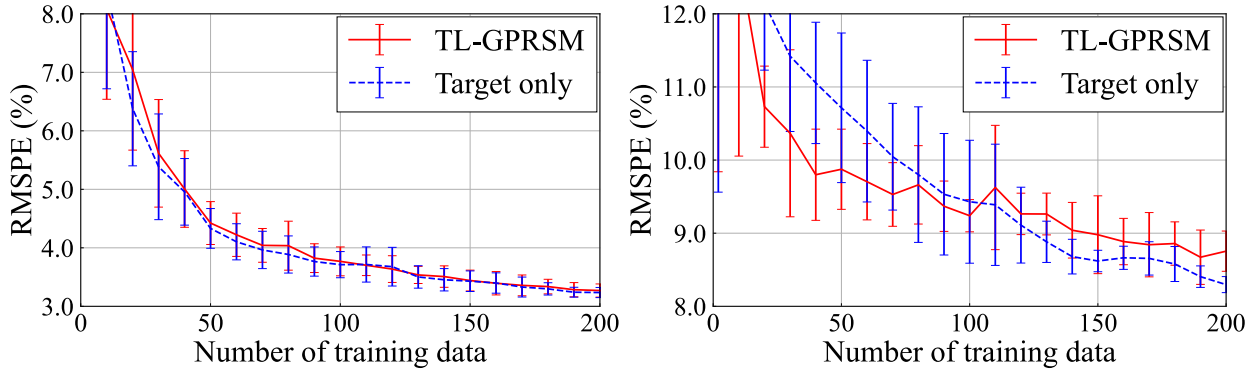

(a) Accuracies of constructed surrogate models (left: pier, right: bearing)

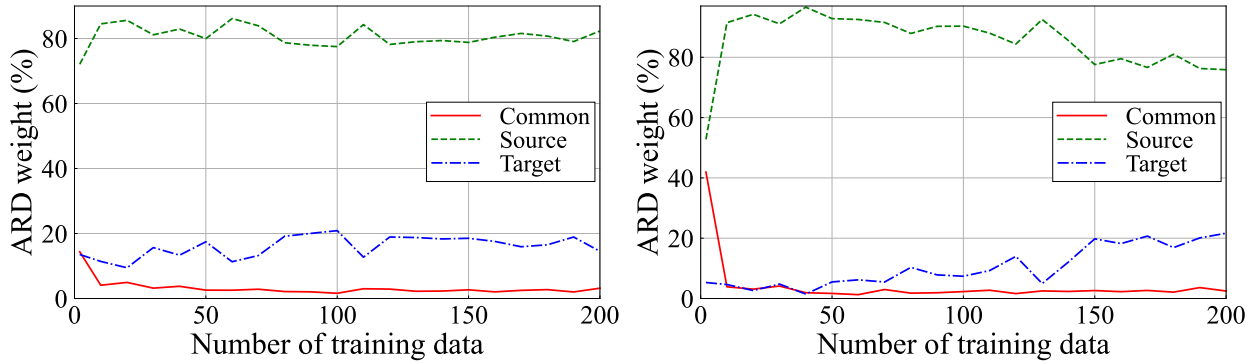

(b) Contributions of common, source, and target domains (left: pier, right: bearing)

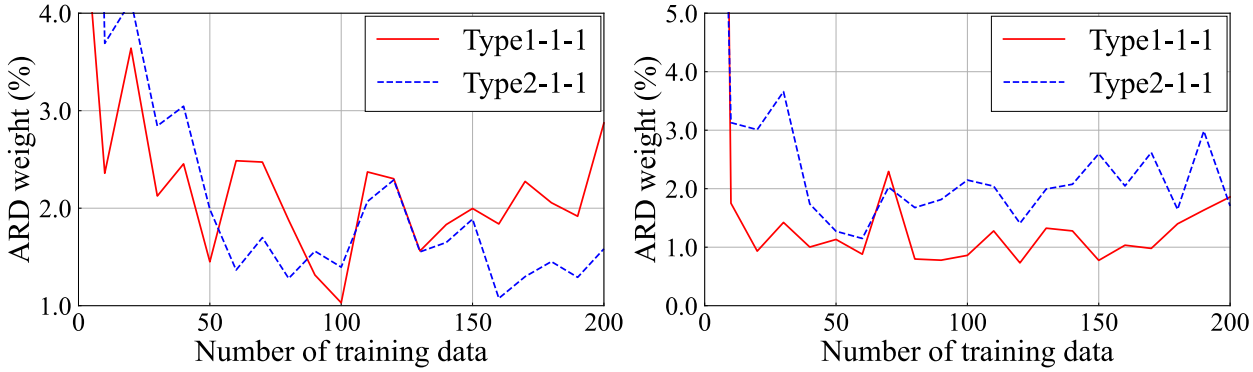

(c) Contribution of common part for each source domain (left: pier, right: bearing)

Fig. 16 Results of surrogate model construction in target domain of KAIHOKUBASHI (Case #3)

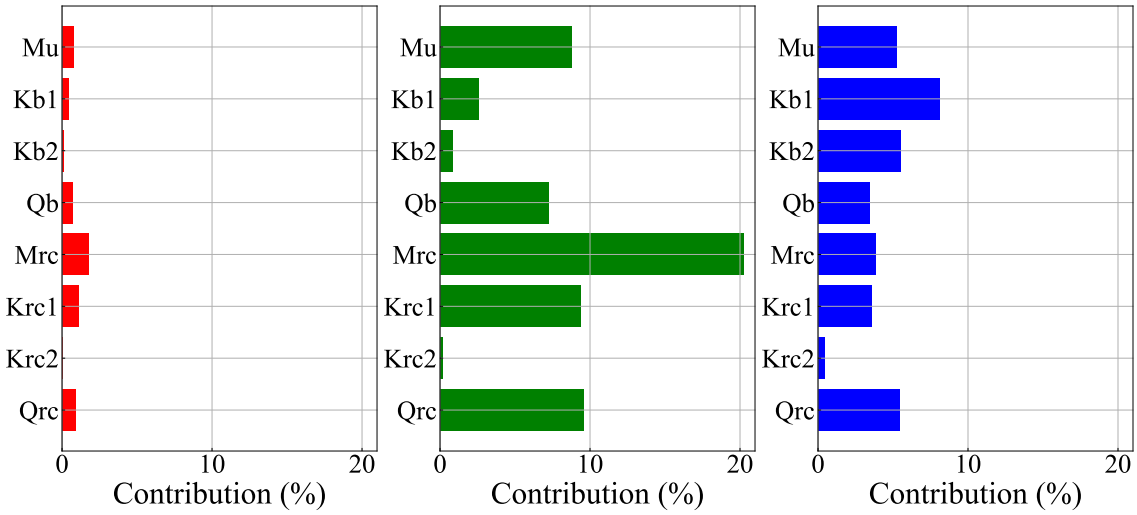

(a) Case #2 JMA KOBE (number of target domain training data: 50)

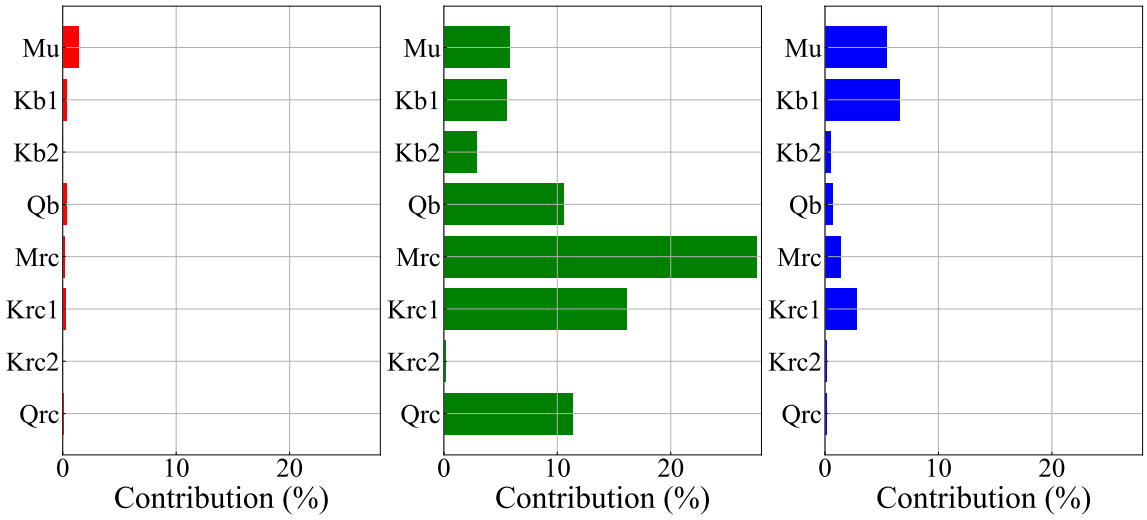

(b) Case #3 KAIHOKUBASHI (number of target domain training data: 50)

Fig. 17 Estimated contributions of model parameter uncertainties to the maximum displacement of the RC pier (Left: Common part, Center: Source part, Right: Target part)

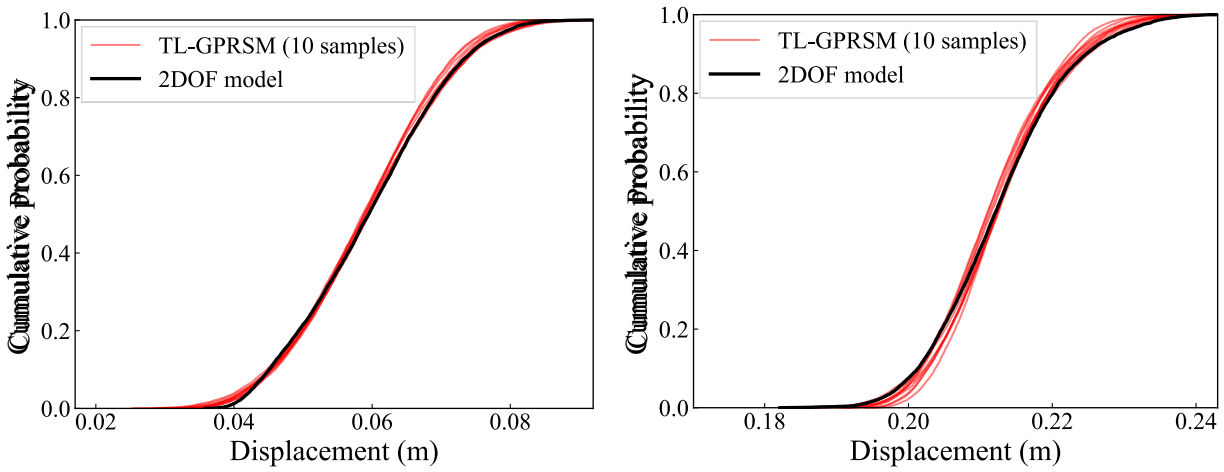

(a) RC pier (b) Rubber bearing

Fig. 18 Prediction of cumulative distribution of output values by TL-GPRSM in Case #2

5. Conclusions

The GPR surrogate model with TL (TL-GPRSM) was proposed in this paper. The computational cost for constructing a surrogate model of the target analysis was reduced by using the data of the input–output relationships of the source analysis with any similarity to those of the target analysis. The use of the ARD kernel in GPR was suggested to evaluate the effectiveness of TL and explainability of the constructed surrogate model. Two case studies were conducted to verify the significance of TL-GPRSM. The conclusions are summarized as follows:

- TL-GPRSM was applied to the surrogate modeling of the live-load performance evaluation of a steel plate girder bridge with corrosion damage by applying the source analysis of the undamaged condition. The prediction error was less than 1% RMSPE when 15 target domain data were used. This is equivalent to the accuracy obtained with 25 target data for the surrogate model without TL, regardless of the number of source data.
- The predicted cumulative distribution of the maximum stress in the TL-GPRSM had less uncertainty and the shape was closer to that obtained with the numerical results than the surrogate model without TL using the same number of target data.
- The TL effect could be determined from the contribution of the common part calculated from the

749 ARD kernel. Transfer learning was determined to be more effective when the number of source data
750 with lower RMSPE was large. Furthermore, ARD made it possible to know the contribution of the
751 individual parameters, and the contribution of parameters related to degradation damage was high.
752 - The seismic performance evaluation of a seismic isolation bridge pier considering the variation in
753 the input earthquake ground motions was the second application considered for verification. This
754 involved the surrogate modeling of nonlinear time-history analysis. It was shown that the
755 effectiveness of TL was not as high as in the linear structural analysis in the first case; however, the
756 TL-GPRSM was able to predict the distributions of the maximum displacements with slightly
757 higher accuracy than the surrogate model without TL in some input cases.
758 - In nonlinear analysis, it was possible to determine the effectiveness of TL based on the magnitude
759 of the contribution of the common part as estimated by the ARD kernel. The contribution of each
760 parameter to the output estimated by the ARD kernel was reasonable from the viewpoint of
761 nonlinear structural dynamics.
762 A future topic of study is the further consideration of surrogate modeling of nonlinear dynamic
763 systems with effective TL. Further, the advanced DoE sampling that takes advantage of the estimated
764 contributions in ARD is expected to reduce the computational cost of creating training data for
765 effective TL. The selection of the kernel function in GPR with ARD is also worth considering, as the
766 computational cost might be reduced by capturing the characteristics of the input–output relationship
767 of the target numerical analysis appropriately. However, the results of this paper showed that the TL-
768 GPRSM was effective in constructing the surrogate model of linear numerical calculations by
769 reducing the computational cost of the structural performance analysis with linear numerical
770 calculation under variation in uncertainties, such as the analysis of the damaged condition based on
771 that of the undamaged initial condition. Moreover, it was shown that the effectiveness of TL in each
772 surrogate modeling and the explainability of the constructed model could be discussed by deriving
773 the contributions of each parameter by using the ARD kernel. This is significant in ensuring the

774 acceptability of the constructed surrogate models in the structural performance evaluation for any
775 decision-making.

776

777 **Funding**

778 This study was supported by the JST FOREST Program, Japan [grant number JPMJFR205T].

779

780 **References**

781 [1] Bucher CG, Bourgund U. A fast and efficient response surface approach for structural reliability
782 problems. Struct Saf 1990;7:57–66. https://doi.org/10.1016/0167-4730(90)90012-E.

783 [2] Kim S-H, Na S-W. Response surface method using vector projected sampling points. Struct Saf
784 1997;19:3–19. https://doi.org/10.1016/S0167-4730(96)00037-9.

785 [3] Zhao W, Qiu Z. An efficient response surface method and its application to structural reliability
786 and reliability-based optimization. Finite Elem Anal Des 2013;67:34–42.
787 https://doi.org/10.1016/j.finel.2012.12.004.

788 [4] Rocco CM, Moreno JA. Fast Monte Carlo reliability evaluation using support vector machine.
789 Reliab Eng Syst Saf 2002;76:237–43. https://doi.org/10.1016/S0951-8320(02)00015-7.

790 [5] Roy A, Manna R, Chakraborty S. Support vector regression based metamodeling for structural
791 reliability analysis. Probab Eng Mech 2019;55:78–89.
792 https://doi.org/10.1016/j.probengmech.2018.11.001.

793 [6] Hawchar L, El Soueidy C-P, Schoefs F. Principal component analysis and polynomial chaos
794 expansion for time-variant reliability problems. Reliab Eng Syst Saf 2017;167:406–16.
795 https://doi.org/10.1016/j.ress.2017.06.024.

796 [7] Marelli S, Sudret B. An active-learning algorithm that combines sparse polynomial chaos
797 expansions and bootstrap for structural reliability analysis. Struct Saf 2018;75:67–74.
798 https://doi.org/10.1016/j.strusafe.2018.06.003.

799 [8] Le V, Caracoglia L. A neural network surrogate model for the performance assessment of a
800 vertical structure subjected to non-stationary, tornadic wind loads. Comput Struct
801 2020;231:106208. https://doi.org/10.1016/j.compstruc.2020.106208.

802 [9] Chojaczyk AA, Teixeira AP, Neves LC, Cardoso JB, Guedes Soares C. Review and application
803 of Artificial Neural Networks models in reliability analysis of steel structures. Struct Saf

2015;52:78–89. https://doi.org/10.1016/j.strusafe.2014.09.002.

[10] Deng J, Gu D, Li X, Yue ZQ. Structural reliability analysis for implicit performance functions using artificial neural network. Struct Saf 2005;27:25–48. https://doi.org/10.1016/j.strusafe.2004.03.004.

[11] Zhou T, Peng Y. Kernel principal component analysis-based Gaussian process regression modelling for high-dimensional reliability analysis. Comput Struct 2020;241:106358. https://doi.org/10.1016/j.compstruc.2020.106358.

[12] Su G, Peng L, Hu L. A Gaussian process-based dynamic surrogate model for complex engineering structural reliability analysis. Struct Saf 2017;68:97–109. https://doi.org/10.1016/j.strusafe.2017.06.003.

[13] Gaspar B, Teixeira AP, Soares CG. Assessment of the efficiency of Kriging surrogate models for structural reliability analysis. Probab Eng Mech 2014;37:24–34. https://doi.org/10.1016/j.probengmech.2014.03.011.

[14] Avendaño-Valencia LD, Abdallah I, Chatzi E. Virtual fatigue diagnostics of wake-affected wind turbine via Gaussian Process Regression. Renewable Energy 2021;170:539–61. https://doi.org/10.1016/j.renene.2021.02.003.

[15] Rasmussen CE. Gaussian Processes in Machine Learning. In: Bousquet O, von Luxburg U, Rätsch G, editors. Advanced Lectures on Machine Learning: ML Summer Schools 2003, Canberra, Australia, February 2 - 14, 2003, Tübingen, Germany, August 4 - 16, 2003, Revised Lectures, Berlin, Heidelberg: Springer Berlin Heidelberg; 2004, p. 63–71. https://doi.org/10.1007/978-3-540-28650-9_4.

[16] Bichon BJ, Eldred MS, Swiler LP, Mahadevan S, McFarland JM. Efficient Global Reliability Analysis for Nonlinear Implicit Performance Functions. AIAA Journal 2008;46:2459–68. https://doi.org/10.2514/1.34321.

[17] Echard B, Gayton N, Lemaire M. AK-MCS: An active learning reliability method combining Kriging and Monte Carlo Simulation. Struct Saf 2011;33:145–54. https://doi.org/10.1016/j.strusafe.2011.01.002.

[18] Gaspar B, Teixeira AP, Guedes Soares C. Adaptive surrogate model with active refinement combining Kriging and a trust region method. Reliab Eng Syst Saf 2017;165:277–91. https://doi.org/10.1016/j.ress.2017.03.035.

[19] Xiao N-C, Zuo MJ, Guo W. Efficient reliability analysis based on adaptive sequential sampling design and cross-validation. Appl Math Model 2018;58:404–20. https://doi.org/10.1016/j.apm.2018.02.012.

[20] Zhou T, Marelli S, Sudret B, Peng Y. AK-PDEMi: A failure-informed enrichment algorithm for improving the AK-PDEM in reliability analysis. Mech Syst Signal Process 2022.

[21] Echard B, Gayton N, Lemaire M, Relun N. A combined Importance Sampling and Kriging reliability method for small failure probabilities with time-demanding numerical models. Reliab Eng Syst Saf 2013;111:232–40. https://doi.org/10.1016/j.ress.2012.10.008.

[22] Huang X, Chen J, Zhu H. Assessing small failure probabilities by AK–SS: An active learning method combining Kriging and Subset Simulation. Struct Saf 2016;59:86–95. https://doi.org/10.1016/j.strusafe.2015.12.003.

[23] Moustapha M, Marelli S, Sudret B. Active learning for structural reliability: Survey, general framework and benchmark. Struct Saf 2022;96:102174. https://doi.org/10.1016/j.strusafe.2021.102174.

[24] Weiss K, Khoshgoftaar TM, Wang D. A survey of transfer learning. Journal of Big Data 2016;3:1–40. https://doi.org/10.1186/s40537-016-0043-6.

[25] Xiong Y, Guo L, Zhang Y, Xu M, Tian D, Li M. Surrogate modeling for spacecraft thermophysical models using deep learning. Neural Comput Appl 2022. https://doi.org/10.1007/s00521-022-07257-7.

[26] Kaya M, Hajimirza S. Using a Novel Transfer Learning Method for Designing Thin Film Solar Cells with Enhanced Quantum Efficiencies. Sci Rep 2019;9:5034. https://doi.org/10.1038/s41598-019-41316-9.

[27] Tian K, Li Z, Zhang J, Huang L, Wang B. Transfer learning based variable-fidelity surrogate model for shell buckling prediction. Compos Struct 2021;273:114285. https://doi.org/10.1016/j.compstruct.2021.114285.

[28] Golparvar B, Papadopoulos P, Ezzat AA, Wang R-Q. A surrogate-model-based approach for estimating the first and second-order moments of offshore wind power. Appl Energy 2021;299:117286. https://doi.org/10.1016/j.apenergy.2021.117286.

[29] Williams C, Rasmussen C. Gaussian processes for regression. Advances in Neural Information Processing Systems 1995.

[30] Wipf D, Nagarajan S. A new view of automatic relevance determination. Advances in Neural Information Processing Systems 2007;20.

[31] Liu DC, Nocedal J. On the limited memory BFGS method for large scale optimization. Math Program 1989;45:503–28. https://doi.org/10.1007/BF01589116.

[32] GPy. GPy: A Gaussian process framework in python since 2012.

869 http://github.com/SheffieldML/GPy.

870 [33] Daumé H III. Frustratingly Easy Domain Adaptation. ArXiv [CsLG] 2009.
871 https://doi.org/10.48550/arXiv.0907.1815.

872 [34] McKay MD, Beckman RJ, Conover WJ. Comparison of Three Methods for Selecting Values of
873 Input Variables in the Analysis of Output from a Computer Code. Technometrics 1979;21:239–
874 45. https://doi.org/10.1080/00401706.1979.10489755.

875 [35] Nishio M, Miura M, Shuku T. Sparse Surrogate Modeling for Structural Reliability Analysis of
876 Existing Bridges. Journal of Japan Society of Civil Engineers, Ser A2 (Applied Mechanics
877 (AM)) 2018;74:I_125-I_136. https://doi.org/10.2208/jscejam.74.I_125. (in Japanese)

878 [36] Japan Road Association. SPECIFICATION FOR HIGHWAY BRIDGES PART II STEEL
879 BRIDGES. Japan Road Association; 2012. (in Japanese)

880 [37] Japan Road Association. Handout on Seismic Design of Road Bridges [Translated from
881 Japanese]. Japan Road Association; 1997. (in Japanese)

882 [38] Takeda T, Sozen MA, Nielsen NN. Reinforced Concrete Response to Simulated Earthquakes.
883 Journal of the Structural Division 1970;96:2557–73. https://doi.org/10.1061/JSDEAG.0002765.

884 [39] Japan Road Association. SPECIFICATIONS FOR HIGHWAY BRIDGES Part V SEISMIC
885 DESIGN. Japan Road Association; 2012. (in Japanese)